Open Access

E&G Quaternary Science Journal

Research article

Multi-method study of the Middle Pleistocene loess–palaeosol sequence of Köndringen, SW Germany

Lea Schwahn[1], Tabea Schulze[1], Alexander Fülling[1], Christian Zeeden[2], Frank Preusser[1], and Tobias Sprafke[3,4]

[1]Institute of Earth and Environmental Sciences, University of Freiburg, Freiburg, Germany
[2]Rock Physics and Borehole Geophysics, Leibniz Institute for Applied Geophysics, Hanover, Germany
[3]Center of Competence for Soils, BFH-HAFL, Zollikofen, Switzerland
[4]Institute of Geography, University of Bern, Bern, Switzerland

Correspondence: Frank Preusser (frank.preusser@geologie.uni-freiburg.de)

How to cite: Schwahn, L., Schulze, T., Fülling, A., Zeeden, C., Preusser, F., and Sprafke, T.: Multi-method study of the Middle Pleistocene loess–palaeosol sequence of Köndringen, SW Germany, E&G Quaternary Sci. J., 72, 1–21, https://doi.org/10.5194/egqsj-72-1-2023, 2023.

Abstract: Loess–palaeosol sequences (LPSs) remain poorly investigated in the southern part of the Upper Rhine Graben but represent an important element to understand the environmental context controlling sediment dynamics in the area. A multi-method approach applied to the LPS at Köndringen reveals that its formation occurred during several glacial–interglacial cycles. Field observations, as well as colour, grain size, magnetic susceptibility, organic carbon, and carbonate content measured in three profiles at 5 cm resolution, provide detailed stratigraphical information. Only minor parts of the LPS are made up of loess sediment, whereas the major parts are polygenetic palaeosols and pedosediments of varying development that are partly intersected, testifying to a complex local geomorphic evolution. The geochronological framework is based on 10 cm resolution infrared-stimulated luminescence (IRSL) screening combined with 18 multi-elevated-temperature post-IR IRSL ages. The luminescence ages indicate that two polygenetic, truncated Luvisols formed during marine isotope stages (MISs) 9(–7?) and MIS 5e, whereas unaltered loess units correspond to the last glacial (MISs 5d–2) and MIS 8. The channel-like structure containing the two truncated Luvisols cuts into > 2 m thick pedosediments apparently deposited during MIS 12. At the bottom of the LPS, a horizon with massive carbonate concretions (loess dolls) occurs, which may correspond to at least one older interglacial.

Kurzfassung: Löss-Paläoboden-Sequenzen (LPS) sind im südlichen Teil des Oberrheingrabens bisher nur unzureichend untersucht, obwohl sie ein wichtiges Element für das Verständnis der Umweltbedingungen darstellen, welche die Sedimentdynamik in diesem Gebiet gesteuert haben. Die Anwendung eines Multi-Methoden-Ansatzes auf die LPS in Köndringen enthüllt, dass diese während mehrerer glazial-interglazialer Zyklen entstanden ist. Die Feldansprache dreier Profile und Laboranalysen in 5 cm Auflösung (Farbe, Korngröße, magnetische Suszeptibilität, organischer Kohlenstoff- und Karbonatgehalt), geben detaillierte Informationen über deren stratigraphischen Aufbau. Nur geringe Teile des LPS bestehen aus Löß, der teilweise durch Hangabschwemmungen geschichtet ist, während der größte Teil aus polygenetischen Paläoböden und Pedosedimenten unterschiedlicher Ausprägung besteht, die sich teilweise überschneiden und von einer komplexen lokalen geomorphologischen Entwicklung zeu-

gen. Der geochronologische Rahmen basiert auf Screening mittels Infrarot-Stimulierter Lumineszenz (IRSL) mit einer Auflösung von 10 cm in Kombination mit 18 Altern, die mit dem Multi-Elevated-Temperature post-IR IRSL Verfahren bestimmt wurden. Die Lumineszenzalter deuten darauf hin, dass die beiden polygenetischen, gekappten Luvisole während der marinen Isotopenstadien (MIS) 9(–7?) und MIS 5e entstanden sind, während die Lösseinheiten dem letzten Glazial (MIS 5d-2) und MIS 8 entsprechen. Die rinnenartige Struktur, welche die beiden gekappten Luvisole enthält, schneidet in > 2 m mächtige Pedosedimente ein, die offenbar während MIS 12 abgelagert wurden. An der Basis des LPS findet sich ein Horizont mit großen Karbonatkonkretionen (Lößkindl), die mindestens einem älteren Interglazial entsprechen könnten.

1   Introduction

While the Late Pleistocene climate and environmental history of Central Europe is reasonably well understood (e.g. Preusser, 2004; Heiri et al., 2014; Stephan, 2014; Lehmkuhl et al., 2016; Stojakowits et al., 2021), the timing and extent of Middle Pleistocene glaciations, as well as the number of and the environmental conditions during interglacial and interstadial phases, are controversially discussed (e.g. Kleinmann et al., 2011; Stebich et al., 2020; Tucci et al., 2021). This is mainly related to difficulties in establishing independent and robust chronological frameworks and applies in particular to the northern Alpine foreland (van Husen and Reitner, 2011; Preusser et al., 2011). In fact, Middle Pleistocene pollen records close to the Alps and in the Upper Rhine Graben (URG), a major sink of Alpine debris during the Quaternary, are rare and largely fragmentary (Preusser et al., 2005; Knipping, 2008; Gabriel et al., 2013).

Loess–palaeosol sequences (LPSs) are frequently found in the area between the realms of the Alpine and Scandinavian glaciations, yet most work during the past decades has focussed on the Late Pleistocene (e.g. Meszner et al., 2013; Lehmkuhl et al., 2016; Moine et al., 2017; Zens et al., 2018; Fischer et al., 2021; Rahimzadeh et al., 2021; Zöller et al., 2022; Schulze et al., 2022) with few sites covering the Middle Pleistocene (e.g. Terhorst, 2013; Sprafke, 2016). Some Middle Pleistocene sites have been dated using thermoluminescence (TL; e.g. Zöller et al., 1988; Frechen, 1992); however, this technique does not correspond to the present state of knowledge, and the reliability of the published ages remains uncertain. Relative chronostratigraphy (pedostratigraphy) is based on a priori assumptions and may give biased results. An example is the LPS Wels-Aschet, where Terhorst (2007) suggests a correlation of five fossil palaeosols with marine isotope stages (MISs) 5, 7, 9, 11, and 13–15 (cf. Lisiecki and Raymo, 2005), with the underlying assumption that Luvisols represent interglacial forest ecosystems that have occurred every ca. 100 000 years in Central Europe (Bibus, 2002). While this chronological assignment was apparently supported by palaeomagnetic excursions observed in this LPS (Scholger and Terhorst, 2013), Preusser and Fiebig (2009) discuss a correlation of three of the fossil Luvisols with the three pronounced warm peaks of MIS 7, seemingly supported by infrared-stimulated luminescence (IRSL) dating. This would result in a different correlation with the MIS record as suggested by Terhorst (2007). However, it is unclear if the IRSL ages could be underestimated due to signal instability and saturation effects.

Buylaert et al. (2009) have introduced an approach that allows the dating range of luminescence to be extended, erasing the unstable IRSL component during a first measurement, followed by collecting a more stable signal during subsequent stimulation at an elevated temperature (see review by Zhang and Li, 2020). This post-IR IRSL (pIR) approach was first applied to the LPS from Austria by Thiel et al. (2011a, b, c) and enabled the dating range to be extended back to about 300 ka. Other studies report reliable ages of up to 700 ka (Zander and Hilgers, 2013; Faershtein et al., 2019). A modified version of the pIR approach was suggested by Li and Li (2011) in which IRSL is subsequently stimulated at increasingly higher temperatures with 50 °C increments. The multi-elevated-temperature (MET) pIR (MET-pIR) approach allows signals with increasing stability at higher temperatures to be analysed but at the cost of bleachability of the signal (Kars et al., 2014). Furthermore, higher stimulation temperatures may also induce changes in sensitivity of the signal that may result in incorrect estimates (e.g. Zhang, 2018).

This article is a contribution towards a broader initiative that aims at improving the understanding of the factors controlling deposition in the URG geosystem during the Quaternary. Besides the effects of local tectonics, changes in climate had a major impact on deposition (Weidenfeller and Knipping, 2009; Gabriel et al., 2013; Preusser et al., 2021), in particular linked to the reoccurring glaciations of the Swiss Alps (Preusser et al., 2011), the Black Forest (Hofmann et al., 2020), and the Vosges (Mercier and Jeser, 2004). LPSs reflect changes in past environmental conditions by shifts between loess deposition, soil formation, and phases of erosion and reworking (Sprafke et al., 2014). In the URG, the accumulation of loess is assigned to cold periods (Hädrich, 1975), when the Rhine and its tributaries were braided rivers, with high debris supply due to increased frost weathering and glacial erosion and high transport potential due to meltwater

discharge. During periods of a warm and humid climate (as today), the Rhine had an anastomosing to meandering character with limited debris transport and practically absent aeolian sediment activity due to widespread vegetation cover (e.g. Andres et al., 2001; Houben, 2003; Erkens et al., 2009; Kock et al., 2009). These two environmental modes can be termed glacial and temperate conditions (the latter including both interglacials and interstadials). Less well understood are the environmental conditions responsible for the phases of erosion and reworking that are observed in many Central European LPSs (Lehmkuhl et al., 2016; Sprafke, 2016; Zöller et al., 2022). Presumably these are related to the presence of flowing water (e.g. sheet wash), but deflation may also play an important role. In both cases, vegetation cover must be very limited.

Despite the prominent loess cover, LPSs from the southern part of the URG (Fig. 1) have seen very limited attention so far, with the most recent systematic studies reaching back to the 1980s (Bronger, 1969, 1970; Guenther, 1961, 1987; Hädrich, 1980; Hädrich and Lamparski, 1984; Zöller et al., 1988). Parallel to the present study, Schulze et al. (2022) investigated the Late Pleistocene site of Bahlingen-Schönenberg using a similar approach as applied here. The site investigated here is situated in the village of Köndringen at the foothills of the Black Forest (Fig. 1) and comprises a complicated succession of discontinuous units, including partly layered loess sediments (sensu Sprafke and Obreht, 2016), palaeosols, and pedosediments, as well as horizons of large carbonate concretions. These features indicate that several glacial–interglacial cycles are recorded in this outcrop but with a major contribution of slope processes leading to erosion and reworking. As a first step to unravel the complex Middle to Late Pleistocene history of the LPS at Köndringen, we focus on refining tools to derive robust stratigraphies and reliable chronologies in a easily accessible part of the outcrop.

Our multi-method approach combines a qualitative field description of the outcrop with high-resolution (5 cm) sediment and soil analyses (grain size, colour, magnetic susceptibility, organic matter, and carbonate content). A particular focus is on establishing a chronological framework by applying the MET-pIR dating approach. In addition, the potential of high-resolution (10 cm) IRSL screening is tested (e.g. Roberts et al., 2009; May et al., 2018), as this simplified procedure with regard to preparation and measurement may provide quick and low-cost semi-quantitative age information. Based on a discussion of the pedosedimentary evolution within the chronological framework, comparisons are drawn to Central European loess records of the Middle Pleistocene, and persistent gaps of knowledge and possible solutions are identified.

2 Study area

Loess deposits in the southern part of the URG are mainly found in hilly landscapes, mostly superimposing pre-Pleistocene layers with varying thickness (Keßler and Laiber, 1991). The LPS of Köndringen (48.13915° N, 7.813025° E; 220 m above sea level, a.s.l.) is located in the Black Forest foothills (Emmendinger Vorbergzone), which represent fault blocks along the eastern fault system of the URG (Fig. 1). The investigated site is situated next to a small triangular hill (Ottenberg), almost 1 km north-east of the river Elz and about 16 km E of the river Rhine. To the west of the main fault, several minor faults divide the foothills into two parts, the eastern "loess hill zone" mainly underlain by limestone and the western part where sandstone also is present; both regions are covered by loess sediment of varying thickness with up to 10–15 m (Hädrich, 1965; Hädrich and Stahr, 2001). According to heavy mineral analyses the source of the loess must have been the floodplain of the Upper Rhine (Keßler and Laiber, 1991), with the thickest accumulation of loess occurring on the adjacent foothills of the Black Forest and on the nearby Kaiserstuhl (hills of volcanic origin in the centre of the URG).

A comprehensive review of LPS in the study region was provided by Guenther (1987), including a schematic sketch showing the stratigraphic subdivision of key sites that all include several interstadial and interglacial palaeosols. According to this study, the most complex LPSs of the region are located in the wider surroundings of Köndringen and comprise up to seven loess units and six well-developed palaeosols. Unfortunately, the majority of outcrops are not easily accessible anymore. The only study including geochronological methods in the region until recently (Zöller et al., 1988) applied TL dating to eight samples taken from the LPS Riegel (Fig. 1b). While TL dating was at an early stage of development at that time, ages of 153 ± 14 and 183 ± 17 ka for loess from below what was interpreted as the Last Interglacial soil (MIS 5e; 115–130 ka; Lisiecki and Raymo, 2005) agree with the expected time frame. Middle Pleistocene ages of the four older palaeosols at Riegel are confirmed by TL ages of 259 ± 26, 254 ± 24, 273 ± 23, and > 390 ka for lower parts of the sequence. These findings indicate that regional LPSs cover more than four glacial–interglacial cycles, motivating an approach with state-of-the-art methods to the easily accessible but as yet unstudied LPS Köndringen.

3 Materials and methods

3.1 Profile description and sampling

The three investigated profiles are located at the north-eastern end of a 400 m long outcrop along Landecker Weg in Köndringen, where a complex succession of partly layered loess sediments of varying thickness intercalated by partly discontinuous pedocomplexes and loess doll horizons are ex-
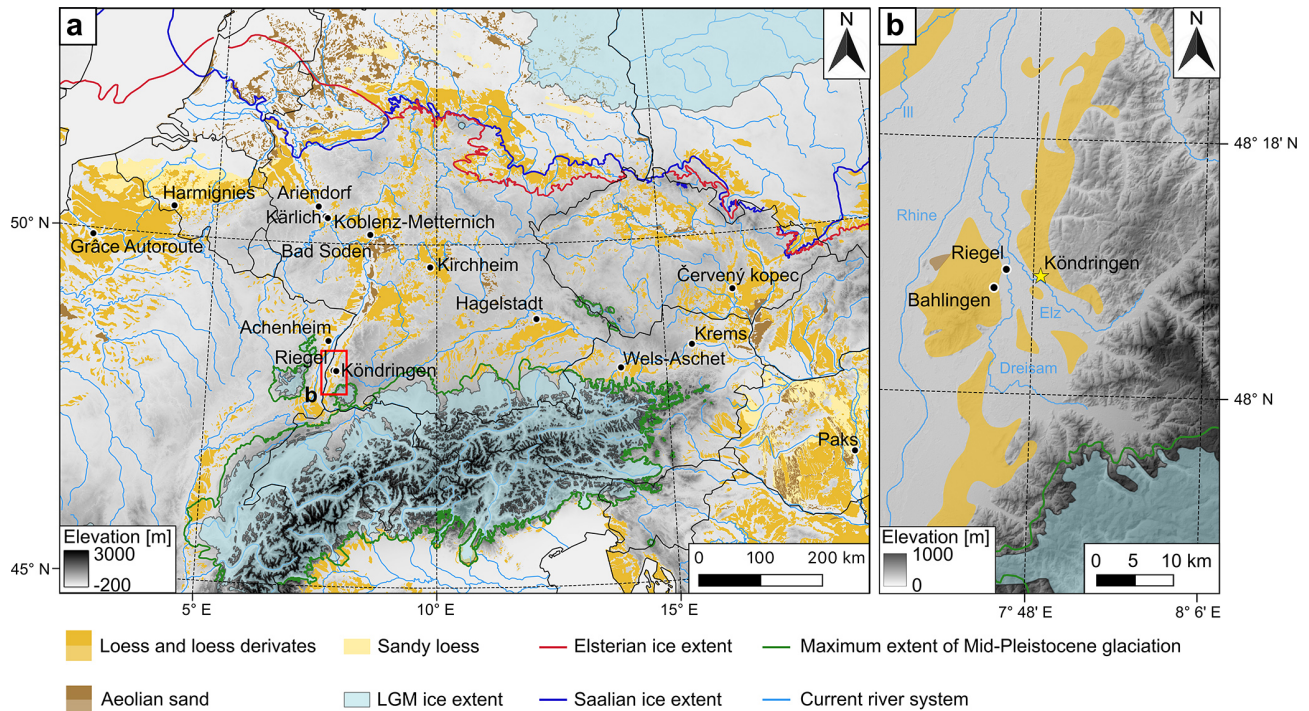
Figure 1. (a) Position of the study area in the Central European loess belt with the location of the mainly Middle Pleistocene LPS mentioned in the text: Grâce Autoroute (Antoine et al., 2021), Harmignies (Haesaerts et al., 2019), Ariendorf (Haesaerts et al., 2019), Kärlich (Boenigk and Frechen, 1998), Koblenz-Metternich (Boenigk and Frechen, 2001), Bad Soden (Semmel and Fromm, 1976), Kirchheim (Rösner, 1990), Achenheim (Junkmanns, 1995), Hagelstadt (Strunk, 1990), Wels-Aschet (Terhorst, 2007; Preusser and Fiebig, 2009; Scholger and Terhorst, 2013), Krems shooting range (Sprafke, 2016), Červený kopec (Kukla, 1977), and Paks (Thiel et al., 2014). **(b)** The investigated profile is situated in the foothills of the Black Forest in the village of Köndringen (yellow star). The digital elevation model data were provided by EEA (2016) and processed with QGIS 3.26. Distribution of aeolian sediments after Lehmkuhl et al. (2021), ice extent after Ehlers et al. (2011), river system from http://naturalearthdata.com (last access: 24 October 2022), and country boundary lines from http://landkartenindex.de (last access: 24 October 2022).

posed. The term loess sediments includes both loess and loess-like sediments (Sprafke and Obreht, 2016). Large parts of the outcrop are covered by a patina, vegetation, or debris, and the site remains protected from spring to autumn due to bird colonies nesting in the cliffs. To capture the main elements of stratigraphy in the most accessible part of the outcrop and to keep disturbance to the minimum, three profiles (KÖN-A, KÖN-B, KÖN-C; Fig. 2) of about 70 cm width were prepared by removing ca. 20 cm of surficial material with spades and scratchers. Colour, structural differences, and specific features were documented qualitatively for a general profile description as the basis for the interpretation of the multi-method dataset. From each profile, samples for determining organic matter and carbonate content, magnetic susceptibility, grain size analysis, and colour measurements were taken at 5 cm resolution as a continuous column (Antoine et al., 2009). Pedological horizon designations based on the qualitative field description and laboratory data (mainly colour data) follow FAO (2006) in the way suggested by Sprafke (2016). Samples for IRSL screening were taken every 10 cm using opaque plastic tubes with a length of 5 cm

and a diameter of ∼ 3 cm, hammered into the freshly cleaned exposure. For luminescence dating, 18 samples were collected in metal tubes with a length of 10–15 cm, hammered into the cleaned profile.

3.2 Colour measurements

Colour measurements were done with a ColorLite sph850 spectrophotometer at the University of Bern that, which allows wavelengths from 400–700 nm to be measured with a spectral resolution of 3.5 nm (Sprafke, 2016). Samples were air-dried and sieved to fine earth (< 2 mm) and measured in a circular field with a diameter of 3.5 mm. The observer angle was 10°, and the light source (six LEDs) corresponds to D65 light. The measuring head was pushed into the loose sample material until it was completely sealed from daylight. Measurements were done at three different sample positions and the results averaged. After stirring the sample, this procedure was repeated, leading to duplicate results. The spectrophotometer was calibrated using a white standard disc after every 10th measurement. The acquired data (various colour variables, remission spectra) were analysed using Microsoft Ex-
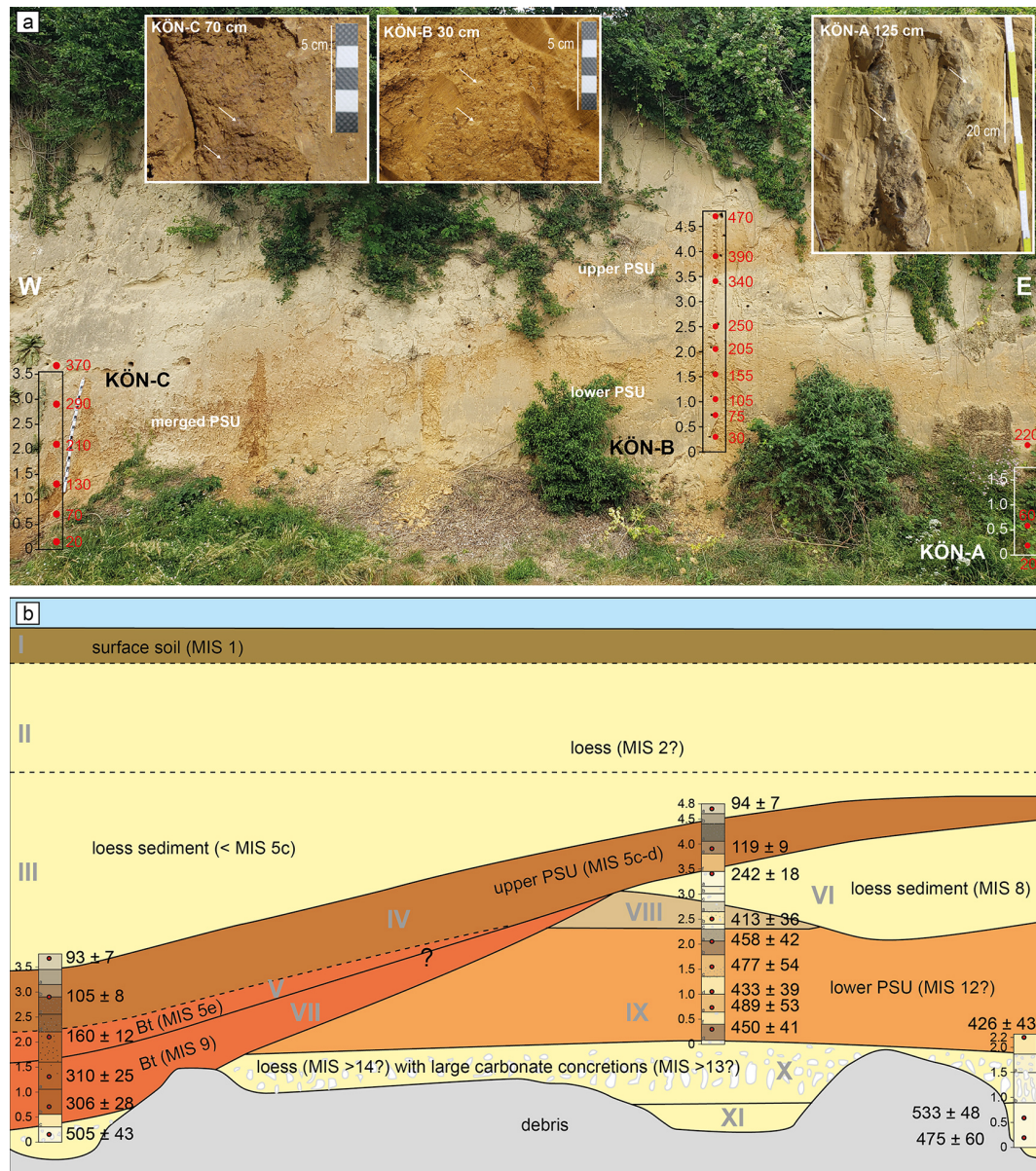
Figure 2. (a) Outcrop photo with the two pedosedimentary units (PSUs) merging into one towards the left hand side and location of three studied profiles KÖN-A (overgrown at moment of photography), KÖN-B, and KÖN-C, with the positions of luminescence samples and their numbers (in red). Rectangles mark the position of the sampling columns. The insets show (from left to right, marked with white arrows) clay coatings in a large crack of weakly developed subsoil of profile KÖN-C (at 70 cm), lenticular structure with silt–loam separation as a result of frost action in the lower part of KÖN-B (at 30 cm), and massive carbonate concretions exposed in profile KÖN-A (at 125 cm). **(b)** The stratigraphic units I–XI shown in the outcrop sketch consider chronostratigraphic relations (MIS after Lisiecki and Raymo, 2005) based on luminescence ages (in black, with uncertainties). Detailed profile sketches are given in Fig. 4.

cel© with the software ColorDaTra 1.0.181.5912. Mean values for each sample were calculated and visualised as real colours based on RGB variables, including two-step RGB tuning, useful to determine subtle colour variations in weakly differentiated LPSs (Sprafke et al., 2020). The L^*-value of the CIELAB colour space represents variations in lightness, whereas a^* corresponds to the intensity of red versus green (> 0 or < 0, respectively) and b^* to the intensity of yellow versus blue (> 0 or < 0, respectively) (Viscarra Rossel et al., 2006).

3.3 Sediment and soil analyses

Grain sizes distributions were measured using a Malvern Mastersizer 3000 laser diffraction spectrometry device (Malvern Panalytical). Samples were dried at 105 °C for at

least 12 h and sieved through a 1 mm sieve (upper effective limit of the device), and 1–2 g was dispersed for 12 h in 50 mL sodium hexametaphosphate (33 g $Na_6 P_6 O_{18}$ and 7 g $Na_2 CO_3$ dissolved in 1 L of distilled water). A similar protocol as used by Abdulkarim et al. (2021) was applied with a particle refractive index of 1.53, a dispersant refractive index of 1.33, an absorption index of 0.01, a stirrer speed of 1660 rpm, and with the ultrasonication off. For every sample five measurements were carried out, and average values were calculated using MATLAB R2021a. The grain size index (GSI: [%20–63 μm] / [% < 20 μm]) was calculated according to Antoine et al. (2009). Clay contents determined by laser diffraction spectrometry for samples from KÖN oscillate around 2 %, which is in disagreement to field-testing trained against classical sedimentation-based methods. Therefore, we assume that the joint clay to fine silt fraction (< 6.3 μm) roughly corresponds to the clay fraction as determined by the classical sieve–pipette analysis. This is in accordance with a large number of studies that confirm a marked difference between the laser diffraction spectrometry device and traditional sedimentation-based methods and suggest the use of alternative boundaries between 4 and 8 μm (mainly depending on soil mineralogy) to translate into "pipette clay" (clay$_p$; e.g. Konert and Vandenberghe, 1997; Antoine et al., 2009).

For the determination of organic matter (C_{org}) and carbonate contents, samples were dried at 105 °C for > 12 h and then pestled with a mortar and sieved to < 2 mm, and about 1 g was used for analyses. In the first cycle, samples were placed in a Nabertherm muffle at 550 °C for 5 h for the determination of organic carbon content (Heiri et al., 2001). Loss on ignition (LOI) was calculated by dividing the dry weight by the weight after the 550 °C burning cycle. However, this value represents double the real organic carbon content (Meyers and Lallier-Verges, 1999), and consequently all values reported have been corrected for this. As C_{org} contents of loess are usually not higher than 0.5 % (Fischer et al., 2021), we must assume that lost interlayer water of clay minerals significantly contributes to the LOI-determined signal. Carbonate contents were subsequently determined using the same material after heating for 3 h at 950 °C (Heiri et al., 2001).

For magnetic susceptibility (weight normalised; χ) measurements, carried out at the Leibniz Institute for Applied Geophysics in Grubenhagen, samples were homogenised and placed in non-magnetic plastic boxes of 6.4 cm^3 so that the material was fixed and could not move. The χ was measured in alternating fields of 505 and 5050 Hz with 400 A m^{-1} using a MAGNON VFSM, providing both low-field χ and frequency dependency of the χ. The χ is here given as weight-normalised, taking weights of samples and boxes into account. Temperature-dependent χ was measured following Zeeden et al. (2021) in an argon atmosphere for nine depth intervals (samples: KÖN-A_20–25, KÖN-A_75–80, KÖN-A_140–145, KÖN-B_85–90, KÖN-B_350–

355, KÖN-C_75–80, KÖN-C_135–140, KÖN-C_225–230, KÖN-C_280–285) using an AGICO CS3 high-temperature furnace.

3.4 Luminescence screening

In the red-light laboratory, the outer ca. 1 cm of the sample material from the light-contaminated ends of the sampling tubes was discarded. Samples were then dried at 50 °C for at least 24 h and gently pestled in a mortar. Part of the material gained this way was fixed on small steel sample discs that were previously coated with a thin layer of silicon oil (6 mm stamp) so that the sample material would stick to the surface during measurement. For each sample, three subsamples were generated and measured on a Lexsyg Smart device (Freiberg Instruments; Richter et al., 2015) with the detection window centred at 410 nm. The measurement protocol comprised the IRSL stimulation of the natural signal (Ln) and that induced by laboratory irradiation (Tn, ca. 22 Gy), both after heating to 250 °C (preheat) and using a stimulation at 50 °C (Table S1 in the Supplement). The ratio Ln / Tn was calculated based on the IRSL emission recorded during the first 20 s of stimulation after subtracting the last 20 s as background.

3.5 Luminescence dating

The sediment from the outer ends of the aluminium tubes was scraped off and used for determining the activity of dose-rate-relevant elements. The remaining material was dried and subsequently treated with hydrochloric acid (20 %) and hydrogen peroxide (30 %) to remove carbonates and organic matter, respectively, each time, followed by rinsing with deionised water. Due to the low sand content of the sediment, the polymineral fine-grain fraction 4–11 μm was separated for equivalent dose (D_e) determination using Atterberg cylinders and centrifuging. The isolated fine-grain material was placed on stainless steel discs by pipetting from a sediment solution in acetone. For measuring the dose rate, samples were dried, homogenised, and subsequently transferred into flat plastic containers (7.5 × 3 cm). After storage for at least 30 d to allow for the establishment of radioactive equilibrium, the activity of uranium, thorium, and potassium were measured using high-resolution gamma ray spectrometry (Ortec high-purity germanium detector).

Measurements for the determination of D_e were carried out using a Freiberg Instruments Lexsyg Smart device (Richter et al., 2015) with an integrated beta source (max activity 7.1 GBq), delivering ca. 0.645 Gy s^{-1} to the sample material in the given geometry (calibration with Freiberg Instruments fine-grain quartz). The MET-pIR protocol originally suggested by Li and Li (2011; see review by Zhang and Li, 2020) was applied using five IRSL steps at progressively higher stimulation temperatures from 50 to 250 °C with a gradual increase of 50 °C (Table S2). The reasoning behind

this procedure is that the stability of the signal increases with temperature, through this eliminating the effect of fading that may lead to the underestimation of feldspar IRSL if not corrected for. Li and Li (2011) report stable signals not affected by fading for stimulation temperatures of 200 and 250 °C. However, it is also known that the time to reset pIR signals during sediment transport requires much longer time periods compared to quartz optically stimulated luminescence (OSL). While the exact time depends on factors such as the transport mechanism and prior dose (Smedley et al., 2015), it has been shown for fluvial settings that pIR ages might significantly overestimate the known age of a sediment (Lowick et al., 2012).

Five to six aliquots were measured for each sample, and the integral 0–15 s of signal readout was used for D_e determination after subtracting the last 10 s as background (Fig. 3a). Dose response curves were fitted using the sum of two exponential growth curves (Fig. 3b). Mean D_e was calculated using the Central Age Model (CAM) of Galbraith et al. (1999; Table S3). A dose recovery test was carried out for sample KÖN-A-20, which revealed recovery ratios within 10 % of unity for all stimulation temperatures but 250 °C. For the latter, the recovery ratio was at 150 %. Problems with high-temperature pIR measurements have also been reported by Li et al. (2018) and Preusser et al. (2021) for fluvial samples from the URG, which are likely related to trap-specific changes in electron trapping probability (see Zhang, 2018; Qin et al., 2018). For some of the pIR-250 measurements aliquots had to be rejected due to saturation effects having been reached, similar to observations by Preusser et al. (2021). All other aliquots passed the usual selection criteria (recycling ratio, recuperation, signal intensity; Wintle and Murray, 2006). Dose rates (Table S4) and ages (Table 1) were calculated using ADELEv2017 software (Degering and Degering, 2020), assuming an a-value of 0.08 ± 0.02 (Rees-Jones, 1995) and an internal potassium content of 12.5 ± 0.5 % (Huntley and Baril, 1997). The water content of all samples was measured after sampling, revealing values between 1.5 % and 14 %, with the majority of values above 10 %. However, since the sediment appeared rather dried out near the surface of the exposure, it is expected that these values significantly underestimate the average sediment moisture during burial. For the dose rate calculations, an average water content of 20 ± 5 % was used. Cosmic dose rates were estimated depending on the geographic position (48.13915° N, 7.813025° E), the altitude (216 m a.s.l.), and the sampling depth following Prescott and Hutton (1994). All ages are reported as kiloyears (ka) before the year of sampling and measurement (2021 CE).
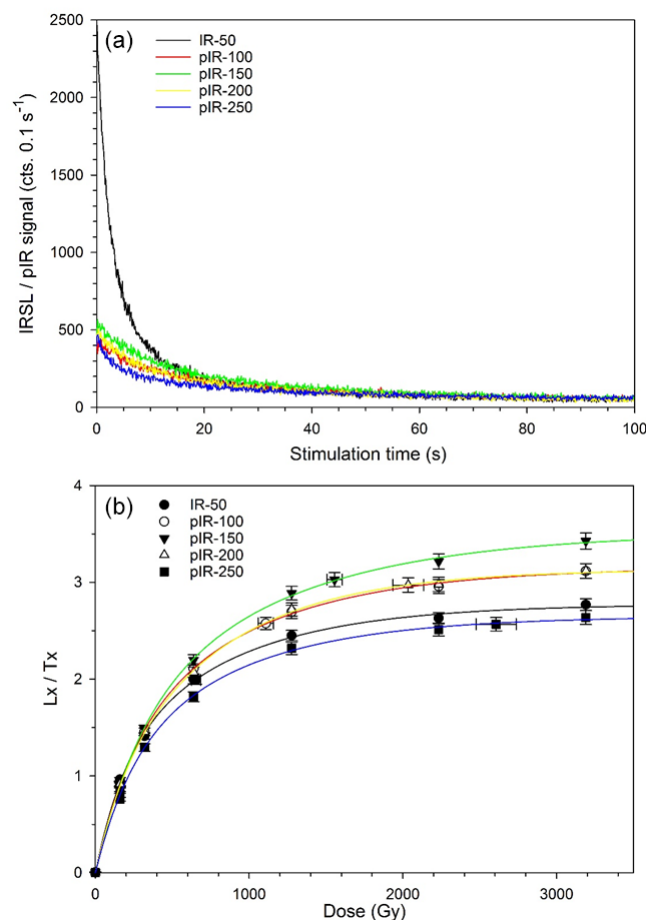

Figure 3. (a) Examples of IRSL decay curves (natural signal) and **(b)** dose response curves for different stimulation temperatures (sample KÖN-C-20; see panel **a** for colour codes).

4 Results

4.1 Profile description

The investigated part of the LPS Köndringen consists of loess and two intercalated brownish pedosedimentary units (PSUs). The ca. 1 m thick upper PSU is inclined to the west, cutting into the underlying loess and merging with the horizontally oriented ca. 2 m thick lower PSU (Fig. 2a). The investigated profiles complement each other to a stratigraphy of 11 units (I–XI; Fig. 2b). Designations of the units V to VIII take into account chronostratigraphic relations revealed by luminescence dating (Fig. 4). Profile KÖN-A comprises the lowermost part of the lower PSU (Unit IX) and a ca. 80 cm thick horizon with thick loess dolls (Unit X; Fig. 2), underlain by calcareous loess (Unit XI). The lower PSU (Unit IX) is exposed in KÖN-B and contains weakly aggregated brownish pedosediments, partly with visible layers and frost features (Fig. 2). In the lowermost and the uppermost parts (units IXg and IXa-c) slightly advanced pedogenic aggregation and pigmentation (pale brown) are visi-

Table 1. Ages determined at 50, 100, 150, 200, and 250 °C using the MET-pIR protocol are shown in kiloyears (ka) before the year of sampling and measurement (2021 CE).

Sample	Depth (cm)	IR-50 (ka)	pIR-100 (ka)	pIR-150 (ka)	pIR-200 (ka)	pIR-250 (ka)
KÖN-C-370	330	53 ± 4	72 ± 5	86 ± 6	93 ± 7	97 ± 7
KÖN-C-290	410	64 ± 5	83 ± 6	97 ± 8	105 ± 8	115 ± 9
KÖN-C-210	490	85 ± 6	120 ± 9	147 ± 11	160 ± 12	180 ± 14
KÖN-C-130	570	122 ± 9	206 ± 16	261 ± 20	310 ± 25	441 ± 63
KÖN-C-70	630	131 ± 9	240 ± 24	314 ± 27	306 ± 28	391 ± 56
KÖN-C-20	680	179 ± 13	310 ± 24	430 ± 34	505 ± 43	441 ± 63
KÖN-B-470	230	53 ± 4	69 ± 5	84 ± 6	94 ± 7	97 ± 7
KÖN-B-390	310	69 ± 5	91 ± 8	111 ± 8	119 ± 9	133 ± 10
KÖN-B-340	360	116 ± 8	170 ± 13	215 ± 16	242 ± 18	267 ± 21
KÖN-B-250	450	160 ± 12	265 ± 21	344 ± 28	413 ± 36	469 ± 50
KÖN-B-205	495	166 ± 13	284 ± 22	373 ± 30	458 ± 42	463 ± 50
KÖN-B-155	545	159 ± 12	294 ± 25	431 ± 40	477 ± 54	457 ± 116
KÖN-B-105	595	148 ± 11	263 ± 20	350 ± 28	433 ± 39	476 ± 57
KÖN-B-75	625	162 ± 12	291 ± 25	388 ± 33	489 ± 53	487 ± 69
KÖN-B-30	670	151 ± 11	282 ± 22	394 ± 32	450 ± 41	529 ± 111
KÖN-A-220	580	135 ± 10	293 ± 24	370 ± 30	426 ± 43	603 ± 106
KÖN-A-60	740	186 ± 14	363 ± 34	466 ± 39	533 ± 48	746 ± 87
KÖN-A-20	780	197 ± 15	353 ± 30	452 ± 38	475 ± 60	581 ± 86

ble. Superimposed is brownish loess with a weak pedogenic structure (Unit VIII) and highly calcareous loess (Unit VI). A clear boundary separates Unit VI from Unit IV, which can be subdivided into a weakly aggregated brown lower part (IVf), grading into a weakly to moderately aggregated greyish-brown upper part (IVa), with a gradual transition into overlying loess sediments (Unit III). Profile KÖN-C starts in the lowermost loess with carbonate concretions (Unit X), ends in the uppermost loess (Unit III), and contains the ca. 3 m thick merged PSU, which is well-aggregated and contains clay coatings in most parts. In Unit VII, clay coatings are mainly found along larger aggregate surfaces and in walls of larger pores, whereas the matrix is mainly yellowish-brown (Fig. 2), grading into more intense brown in the upper part (VIIa). By contrast, Unit V is reddish-brown throughout, with numerous clay coatings and some Mn oxides on ped surfaces. Contrary to KÖN-B, Unit IV in KÖN-C is more homogenous, with moderate aggregation and incipient clay coatings in the lower half (IVc–d). The transition into the overlying greyish, partly layered loess (Unit III) is sharp. Units II and I are not investigated due to accessibility problems and correspond to the uppermost, apparently homogenous loess and the present-day surface soil, respectively.

4.2 Colour

Measured colours allow for a rather robust separation of the sequence into subunits (labelled a, b, etc.) shown in Fig. 4. Colour variations in KÖN-A are minimal there is a slight increase in brownish hue in the uppermost part (Unit Xa), indicated by slightly increasing red (a^*) and yellow (b^*) colour components. The lower PSU in KÖN-B is subdivided into light brown to brown units. The incipient palaeosols in the bottom and upper part are darker (lower L^*) and more brownish (higher a^* and b^*), respectively. The uppermost unit (IXa) is again darker, with a less brownish component. From Unit VIII to VI the a^*- and b^*-values strongly decrease, along with an increase in lightness (L^*). Noticeable are a slightly dark (VIIIa) horizon and another slightly more brownish horizon (VIb). The lower half of the upper PSU has high a^*- and b^*-values, whereas in the upper part, the yellowish component decreases rapidly, and darkness stays high, resulting in a greyish-brown colour. In the merged PSU of KÖN-C L^* remains low, whereas a^* and b^* show a comparable (e.g. common increase in the lower part of VII) but partly deviating pattern. We highlight the peak of a^* in Unit V, whereas the peaks of b^* are shifted to the transition into Unit VII. In Unit IV of profile KÖN-C there are little changes in colour, different to profile KÖN-B, the unit of which is two parts.

4.3 Grain size composition

The texture of the LPS Köndringen is largely dominated by medium to coarse silt (Fig. 4). The loess between the two PSUs of KÖN-B (Unit VI) exhibits a clear mode at the medium–coarse silt boundary (20 µm). By contrast, the mode in the merged PSU (units V and VII) oscillates within the medium silt fraction and is less pronounced due to a wider distribution of grain sizes, specifically towards the finer fractions. The upper PSU in KÖN-B has a granulometry quite similar to the underlying loess, whereas the lower PSU has a
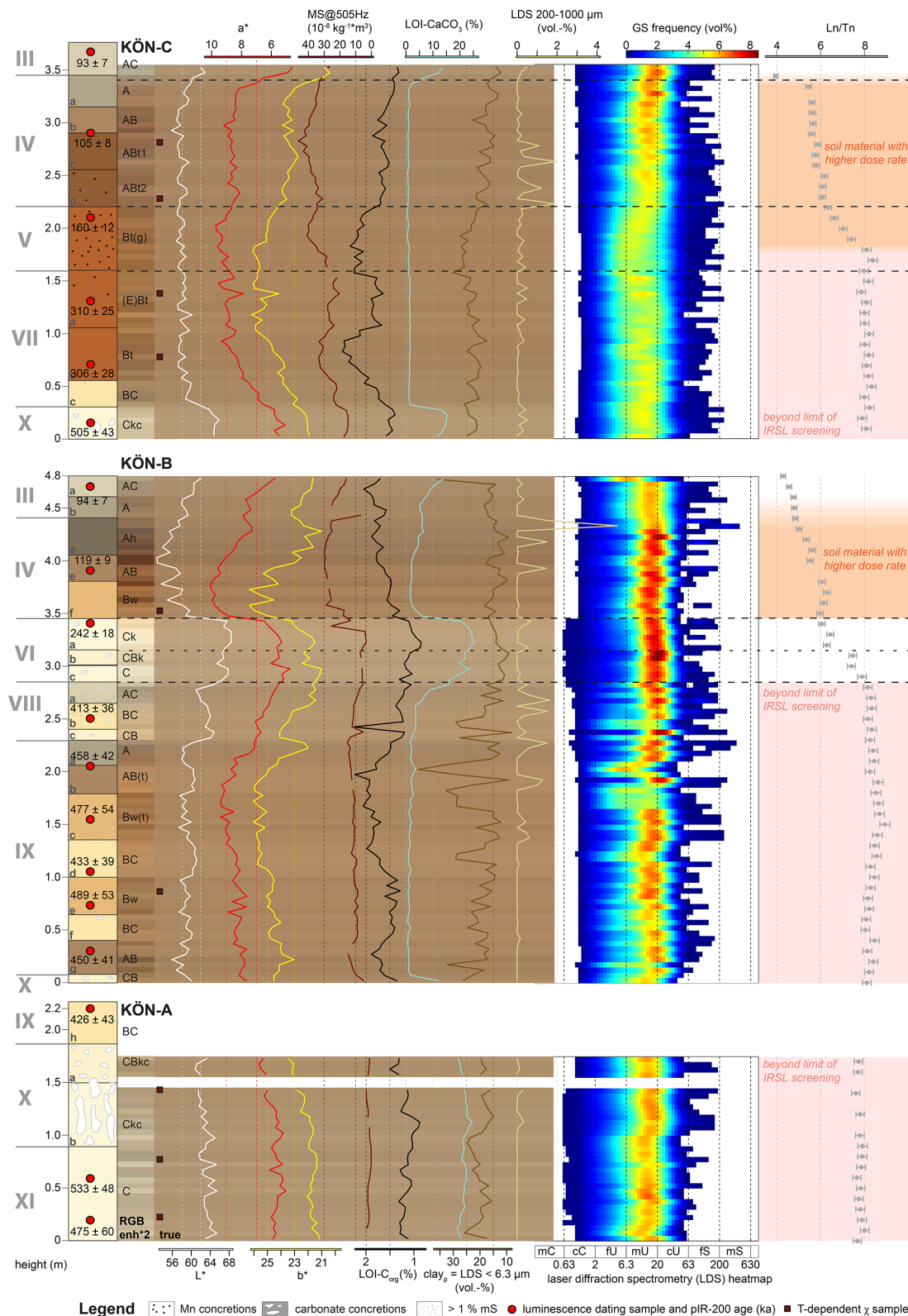
Figure 4. Stratigraphy and laboratory data of the profiles KÖN-A, KÖN-B, and KÖN-C. Real and two-times-enhanced (to the left) RGB colours of each sample are shown as background to the data plots and pedological designations, respectively. Grain size distributions are displayed as heat maps (Schulte and Lehmkuhl, 2018). Ln / Tn ratios are partly beyond the limit of this method (pale red background) or from palaeosols (pale orange background) with a higher dose rate, which is related to the enrichment of clay in such layers. Raw data are available in the Supplement.

variable pattern, with considerable oscillations in the grain size mode, especially in the upper part (VIII and IXa–b). There, more than 1 % medium to coarse sand grains are present; similar peaks are observed in the upper half of the upper PSU (units IVa–b) and the upper half of the merged PSU in KÖN C (units IVc–d).

The loess sediment (Unit VI) between the PSU of KÖN-B contains mostly less than 15 % clay$_p$, whereas the lowermost loess (Unit X–XI) has 15 %–25 % clay$_p$. The upper PSU (Unit IV) has only slightly higher clay$_p$ contents compared to the underlying loess (Fig. 4). The lower PSU (Unit IX) exhibits strong oscillations of clay$_p$ contents in the upper half (occasionally larger than 25 %), where we also noted variable grain size modes and the presence of medium to coarse sand. The merged PSU in KÖN-C has clay$_p$ contents of around 25 % in the well-developed palaeosol units V and VII and 15 %–20 % clay$_p$ in the superimposed horizons (IV).

4.4 Carbonate content, organic carbon, and magnetic susceptibility

The loess between the two PSUs in KÖN-B (Unit VI) and the lower loess (units X–XI) mostly have carbonate contents > 15 %, whereas the merged PSU is completely decalcified (Fig. 4). The upper PSU (Unit IV) contains a few percent of carbonate, which constantly increases to > 15 % in the overlying loess (Unit III). As visible in the field, the transition of Unit IV to Unit III is sharp in KÖN-CA. The lower PSU is almost free of carbonate, with minor contents in those parts with a very variable granulometry (units IXa–b and VIII). In Unit VIIIa, there is a constant increase to 15 % towards the upper unit boundary.

LOI C_{org} contents vary between 1 % in loess and 2 % in the palaeosols and likely represent a mixed signal of organic carbon and clay mineral interlayer water (see Sect. 3.3). Clear peaks in the Bt horizons of the merged PSU (units VIIb and V), high LOI C_{org} contents in the upper half of Unit IX, and some local peak in IXg, which was interpreted as weak palaeosol (Fig. 4), are present.

Mass-specific χ values vary from 10 to 46×10^{-8} m^3 kg^{-1}. Generally, χ and magnetic enhancement of the frequency dependency is comparable to other loess localities in Eurasia (Fig. 5a–b; e.g. Zeeden et al., 2016; Zeeden and Hambach, 2021). The loess units at the bottom of the sequence (IX and X) and between the two PSUs (Unit VI) show distinctively lower χ, which are in a similar range as the χ from the nearby last glacial LPS Bahlingen-Schönenberg (Schulze et al., 2022). The lower PSU in profile KÖN-B shows slightly enhanced χ, with local maxima in the lowermost and uppermost parts of Unit IX and in Unit VIII. The merged PSU in KÖN-C shows the highest χ and also the highest magnetic enhancement. Distinct peaks in the Bt horizons coincide with those of LOI C_{org}. The maximum χ values occur in Unit IV and are considerably higher compared to Unit IV in KÖN-B.

The temperature-dependent magnetic susceptibility properties of nine samples are rather complex and vary considerably within the profile. The results cluster in four groups, described by their heating curves (Fig. 5c–f). All samples show an increase in χ at ca. 325 °C and a subsequent decrease towards ca. 500 °C. Furthermore, samples KÖN_A_20–25 and KÖN_A_75–80 (Fig. 5c) show a weak increase until ca. 570 °C before a sharp decrease until 600 °C. Thereafter, χ continues to decrease until ca. 700 °C. The susceptibility reaches values much higher (ca. 9-fold) during cooling than during the heating process. Samples KÖN_B_85–90 and KÖN_C_135–140 (Fig. 5d) show a further decrease in χ during heating with a steep drop at ca. 590 °C. These samples show only slightly higher χ during cooling than during heating. Samples KÖN_A_140–145, KÖN_B_350–355, and KÖN_C_75–80 (Fig. 5e) show a similar pattern as the first group (Fig. 5a) but have a much more pronounced maximum of χ at ca. 570 °C during heating. The susceptibility during cooling is only ca. 3-fold higher than during heating. Samples KÖN_C_225–230 and KÖN_C_280–285 (Fig. 5f) show a rather constant decrease in χ from ca. 300 °C until ca. 600 °C, as well as a clear further decrease in χ until ca. 700 °C.

4.5 IRSL screening

Ln / Tn values in units X and XI of KÖN-C are very consistent with an average of 7.8 ± 0.2 (Fig. 4). In the upper parts of KÖN-B (units X to VIII) and KÖN-C (units X, VIII, VII), average Ln / Tn values of 8.36 ± 0.26 and 8.08 ± 0.24, respectively, are observed. In KÖN-B, the lower part of Unit VI has an average value of 7.59 ± 0.46, whereas the upper part and that continuing into the lower part of Unit IV show a significantly lower value of 6.20 ± 0.35. In the highest part of the sequence investigated here, the mean Ln / Tn value decreases from 6.07 ± 0.14 (380 cm; Unit IVf) to 4.30 ± 0.11 (480 cm; Unit IIIa). In KÖN-C, Unit V shows a gradual decrease in values from ca. 8.14 ± 0.41 (160–180 cm) to 6.16 ± 0.16 (230 cm). These values continue in Unit IVd (mean 6.01 ± 0.26), whereas Unit IVc has a slightly lower mean value of 5.72 ± 0.24. Units IVb and IVa have similar values (mean 5.61 ± 0.10) but the uppermost sample of Unit IVa is slightly lower (5.43 ± 0.14). Significantly lower is the value of the single sample taken from Unit III (3.93 ± 0.11).

4.6 Luminescence dating

The MET-pIR results in five ages per sample (Table 1), which are expected to reflect an increasing stability of the IR-stimulated signal with increasing stimulation temperature. In fact, this trend is clearly observed for the samples investigated here, as shown in Fig. 6a. On average, the pIR-50 ages are at the ratio 0.42 ± 0.09, the pIR-100 ages at 0.69 ± 0.07, and the pIR-150 ages at 0.88 ± 0.06 of the pIR-200 ages that
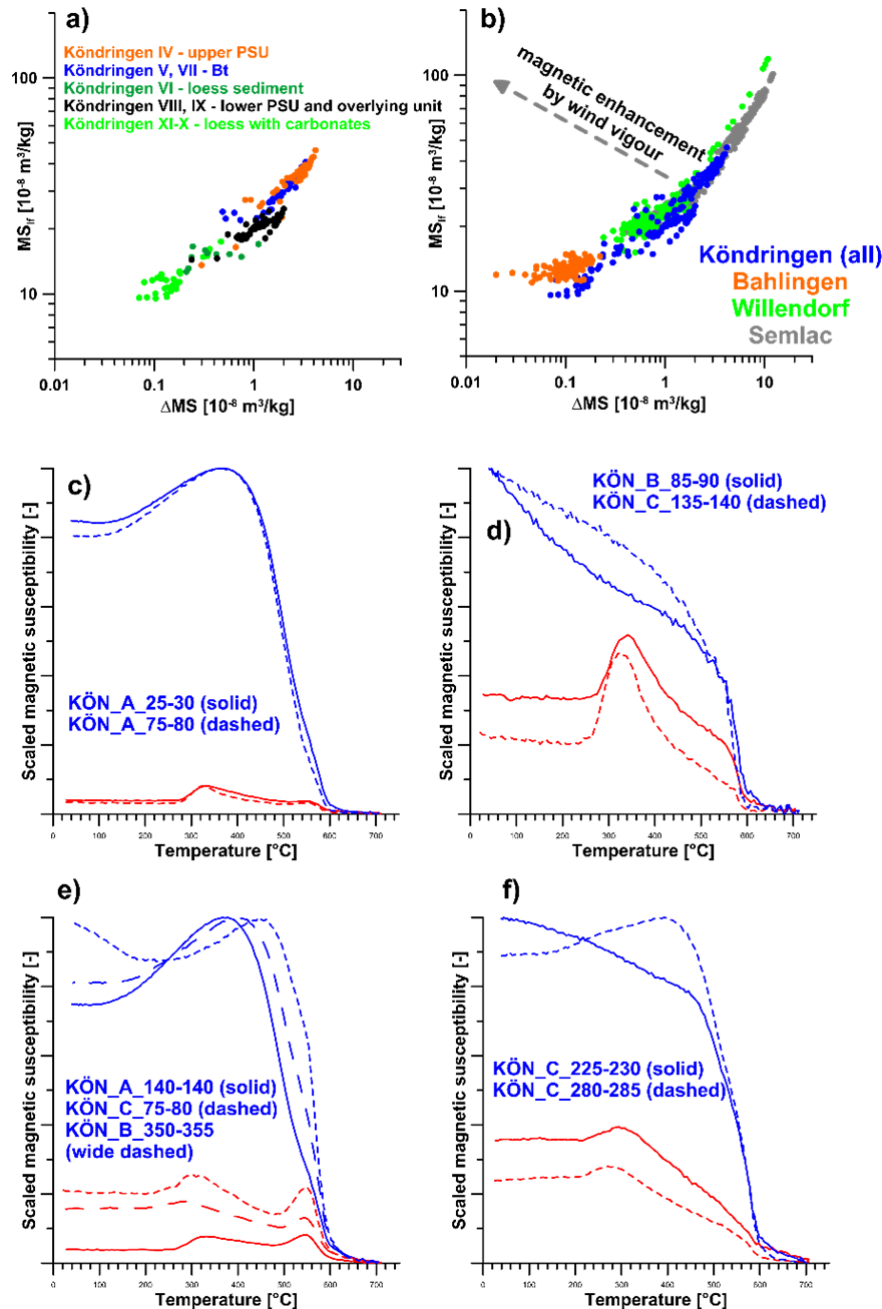
Figure 5. (a) Plot of the magnetic susceptibility (ordinate) and its frequency dependency (in %, abscissa) for different stratigraphic units. **(b)** Comparison of the magnetic susceptibility and its frequency dependence on Bahlingen-Schönenberg, Willendorf, and Semlac (Schulze et al., 2022; Zeeden et al., 2016; Zeeden and Hambach, 2021). This shows that the magnetic properties from Köndringen are in line with other available datasets from Eurasia. Strong indications of either wind vigour or dissolution effects are not present. **(c–f)** Temperature-dependent susceptibility during heating (red) and cooling (blue) of the samples indicated in the figure.

are used as reference. The pIR-250 ages are slightly higher (1.14 ± 0.16). The increase in stimulation temperature goes along with an increase in sensitivity change with the single aliquot regenerative dose (SAR) protocol (Fig. 6b), which is in particular strong for pIR-250 and partly leads to poor recycling ratios. Furthermore, there is a clear difference in the shape of dose response curves, with a flatter shape observed for pIR-250. The latter causes a lower saturation dose for pIR-250. In combination with the observation of highly overestimating dose recovery tests, the pIR-250 ages are considered unreliable, and the discussion of the age of the deposits will rely on the pIR-200 ages (Figs. 2 and 4).
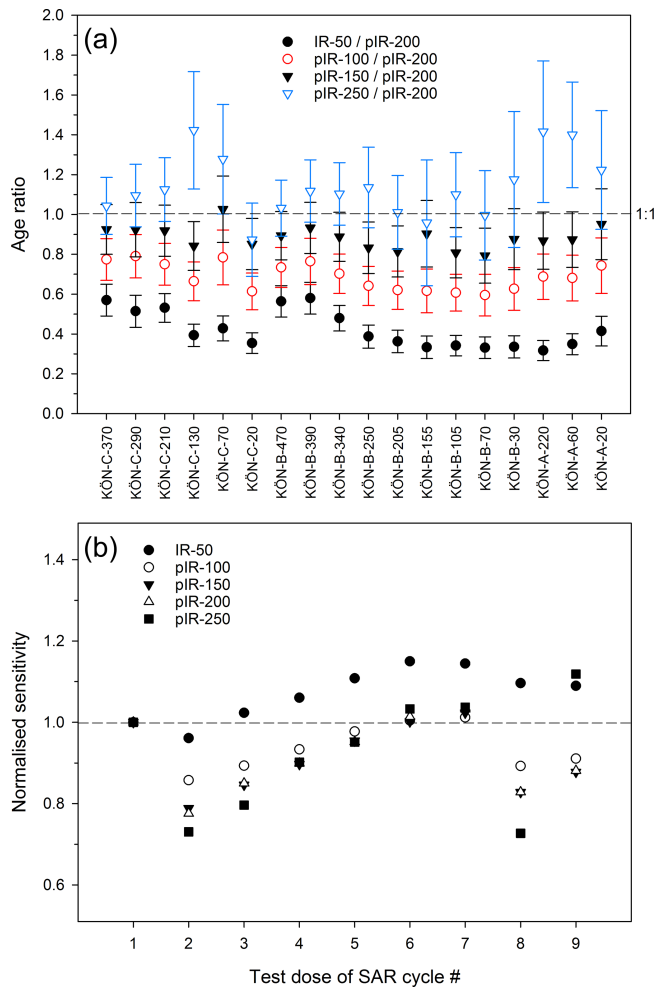
Figure 6. (a) The plot of IRSL and pIR ages determined for different stimulation temperatures normalised against the pIR-200 age demonstrates that ages systemically increase with stimulation temperature. **(b)** The test dose sensitivity change during the course of the SAR cycle for different stimulation temperatures normalised to the first measurement (sample KÖN-C-20) is increasingly larger for higher stimulation temperatures.

5 Discussion

5.1 LPS forming processes

The stratigraphically lowest sediment is pale yellow calcareous loess with a carbonate content of around 20 % and a clear texture mode in the medium to coarse silt fraction (ca. 20 µm; Fig. 4). With few exceptions, this mode is present throughout the LPS, which indicates that loess sediments are the parent materials of all palaeosols in the case the latter did not form from pedosediments. The high content of primary carbonate in unaltered loess reinforces earlier notions that sediment brought by the river Rhine, originating from the largely calcareous northern Swiss Alps and the Jura Mountains, must be a major source of the silt (Hädrich, 1975). Compared to

last glacial loess of the nearby LPS Bahlingen (Schulze et al., 2022) and other last glacial LPSs from Central Europe, for example, Remagen, Garzweiler, and Krems-Wachtberg (Sprafke et al., 2020), which have grain size modes around 40 µm, the grain size mode at Köndringen is ca. 15–20 µm finer. Regionally distributed data on loess granulometry are not available to clarify if our data reveal deviating silt transport regimes during the Middle Pleistocene or if there is a regional differentiation in grain sizes due to transport distances and topographic barriers between the Rhine and Köndringen; it is planned to investigate this in future studies.

In last glacial LPSs with weak pedogenic differentiation, grain size variations are powerful proxies to reconstruct sedimentation dynamics, resulting from catchment geomorphic processes and wind regimes in reaction to past climate change (Antoine et al., 2009; Vandenberghe, 2013; Schulte et al., 2018; Sprafke et al., 2020). At Köndringen, the three profiles encompass mainly pedosedimentary units and well-developed palaeosols. Here, the wider grain size distribution, including increases in the clay fraction, mainly reflects the effect of post-sedimentary alteration, i.e. pedogenesis (Schulte and Lehmkuhl, 2018). Additionally, the reworking of loess and soil material by slope wash may lead to the admixture of coarse components in the case these are exposed further upslope (Sprafke et al., 2020). As the fraction above 1 mm was not determined quantitatively, we use the fraction 200–1000 µm as proxy for slope wash. Peaks are observed in the upper parts of the PSUs, which reflects a typical phenomenon in Central European LPSs, i.e. landscape degradation and slope processes at the transition of warm and moist to cold and dry environmental conditions (e.g. interglacial to glacial transitions) interrupted by phases of weak to moderate pedogenesis (Semmel, 1968; Bibus, 1974; Terhorst et al., 2002; Sprafke et al., 2014).

Landscape stability results in the alteration of loess and slope deposits by pedogenesis with weathering intensity being mainly a function of duration and humidity. Initial terrestrial (well-aerated) pedogenesis in the presence of sufficient soil moisture leads to organic matter accumulation by humification (darkening) and structural changes by bioturbation, followed by decalcification and oxidation (brownish to reddish pigmentation). In addition to pedogenic structuring (aggregation), pigmentation, and increases in χ, advanced soil development leads to increases in clay content due to silicate weathering of silicates and clay translocation, which mainly takes place in interglacials. Clay translocation in Central European loess may also occur during marked interstadials, usually in the presence of pre-weathered pedosediments (Frechen et al., 2007).

At Köndringen, we observe two major PSUs (Fig. 2; KÖN-B profile) merging into one (KÖN-C profile), with specific properties related to pedogenesis and posterior reworking. All PSUs are largely decalcified, the colours are brown, and clay contents are 5 %–15 % higher than the loess in between (Unit VI), reflecting at least moderate pedogenesis.

Clay coatings on polyhedral ped surfaces in units V and VII indicate long-term pedogenesis, likely under interglacial conditions (Semmel, 1968; Terhorst et al., 2002). The two peaks in LOI C_{org} (Fig. 4) coincide with horizons enriched in illuvial clay, as this method is sensitive to minerals with interlayer water. In the field, illuvial clay of Unit V appears to reach into the upper parts of Unit VII, which itself may be a former eluvial horizon of an older Luvisol. Superimposed on the two well-developed palaeosols is a more humic palaeosol with incipient clay coatings, which may correspond to reactivated illuvial clay from pedosediments (Unit IV). High χ values characterise the merged PSU, with peaks corresponding to the Bt horizons (units V and VII) and maxima in the humic horizons of unit IV. This suggests that χ is sensitive to subsoils of truncated to full interglacial palaeosols but even more to preserved humic topsoils, where biochemical processes occur with high intensity.

The χ values of loess at Köndringen and Bahlingen (Schulze et al., 2022) are rather low; only in units affected by advanced pedogenesis do χ values reach those of other European reference profiles (Fig. 5b). As contents of non-magnetic carbonate are similar (ca. 15 %–25 %) in loess of the URG and the Danube Basin (Sprafke, 2016; Pécsi and Richter, 1996), lower χ values of URG loess are possibly related to a higher share of coarse diamagnetic silicate minerals (e.g. quartz). The basal loess at Köndringen has the lowest χ values due to the additional contribution of (non-magnetic) secondary carbonate visible in the field. The thick carbonate concretions below and the brown colour of the lower PSU (Unit IX) give the impression of long-term pedogenesis. However, χ values of the lower PSU are rather low, indicating a weak to moderate intensity of soil formation or a mix of soil and loess material. Granulometric fluctuations in the upper part and layering, frost features, and the weak pedogenic structure in the lower part of the lower PSU (Fig. 2a) support that it consists mainly of reworked soil material. Some re-established pedogenic structure and slight increases in χ in the lowermost part (IXg) and upper part (IXa–c) of the lower PSU indicate weak to moderate pedogenesis of interstadial intensity. Specifically, Unit IXa may correspond to a humic topsoil formed during this interstadial-type pedogenesis. Unit VIII represents enhanced aeolian sedimentation, with Unit VIIIb likely representing a phase of weak pedogenesis, indicated by lower carbonate contents and a more brownish colour.

We interpret the temperature-dependent susceptibility properties (Fig. 5c–f) as indicative of relevant contributions of magnetite, maghemite, and hematite. For Eurasian loess, the increase in χ at $\sim 300\,°C$ has been related to the alteration of weakly magnetic Fe phases to maghemite or magnetite; the heating curves of the magnetic susceptibility plotted in Fig. 5e are most typical of last (inter-)glacial European palaeosols and loess sediments (see Zeeden and Hambach, 2021, and references therein). The drop in the susceptibility at $\sim 585\,°C$ likely represents the Curie temperature of magnetite. The further decrease in the χ towards $700\,°C$ is interpreted as a contribution of hematite (Fig. 5f). While for all samples an increase in χ at $\sim 300\,°C$ is present (Fig. 5c–f), samples shown in Fig. 5c and d show this phenomenon most prominently. For the samples from units X and XI (Fig. 5c), this is not surprising as these are from typical loess, which will easily form magnetic minerals when heated. The much higher susceptibility during cooling for some samples (Fig. 5c) implies that non- or weakly magnetic iron phases are prominently present in the sediment. The susceptibilities that are not much higher during cooling for samples from Unit VIIa (merged PSU) and Unit IXe (lower PSU; Fig. 5d) are interpreted as originating from mature, likely interglacial soils. The absence of strong ferrimagnetism in the lower PSU can be explained by the removal of the very fine fraction during slope wash that led to the reworking of a previously present interglacial soil. The upper PSU in KÖN-B corresponds stratigraphically to the upper part of the merged PSU in profile KÖN-C. Yet, our data show that Unit IV has different properties in both profiles. For KÖN-C, please note the presence of a humic palaeosol with incipient clay illuviation cut sharply by overlying loess. In KÖN-B there is a clear subdivision into a brown, weakly aggregated part and a darker, moderately aggregated part, grading into overlying loess. It is likely that units IVe–f correspond to brown pedosediment which was overprinted by a humic palaeosol and successively buried by loess. The presence of carbonate in the pedosediment indicates that decalcification, allowing for clay illuviation (as in KÖN-C), was not reached in this part of the LPS, but micromorphological studies are necessary to support or neglect this hypothesis (cf. Sprafke et al., 2014). Units IVb–d instead are decalcified and have high χ values, indicating that pedogenesis was stronger. The hematite contribution, seen best in samples from the base of the upper PSU (units IVc, d; see Fig. 5f), implies that the upper PSU contains material from a mature, likely interglacial soil. As for the lower PSU, this phenomenon may be related to the incorporation of older pre-weathered material, which is typical of early glacial palaeosols in Central Europe (Frechen et al., 2007; Sprafke et al., 2014).

Overall, our colour, granulometry, magnetic susceptibility, and LOI data considerably support the subdivision and interpretation of the studied LPS (Fig. 4), although we note that the interpretation appears partly ambiguous in the absence of detailed macro- and micromorphological studies (cf. Sprafke et al., 2014; Sprafke, 2016). As the focus of this study was the testing of new methods, specifically luminescence screening and advanced dating protocols, we note a shortcoming in (micro-)structural information to precisely reconstruct the formation of this complex LPS.

5.2 Chronostratigraphy

Sections KÖN-A and KÖN-C comprise the oldest stratigraphic units (XI and X) for which consistent ages

of 533 ± 48 ka (KÖN-A-20), 475 ± 60 (KÖN-A-60), and 505 ± 43 ka (KÖN-C-20) have been determined. Assuming the two units (XI and X) are quasi-synchronous allows a mean age of 505 ± 71 ka (CAM) to be calculated for the basal part of the investigated sequence. The large uncertainty does not allow an unambiguous correlation with MIS stratigraphy (Lisiecki and Raymo, 2005), but assuming the loess was deposited during a glacial period makes MIS 14 (563–533 ka) and MIS 12 (478–424 ka) the most likely candidates. However, it is at present not known if the pIR-200 ages are affected by systematic underestimation due to, for example, a low level of fading or the onset of signal saturation. The question of potential underestimation can only be answered by comparison with independent age control, which is so far not available for the region. In the absence of any evidence pointing towards age underestimation, the pIR-200 ages are considered reliable for the time being.

In Profile KÖN-A, unit X with massive loess dolls is overlain by pedosediments corresponding to the lowermost part of the lower PSU (Unit IX). The age of 426 ± 43 ka (KÖN-A-220) corresponds to late MIS 12 or early MIS 11. In section KÖN-B, Unit IX contains five superimposed pIR-200 ages overlapping within uncertainties (Table 1, Fig. 5), which represent a mean (CAM) age of 458 ± 21 ka and hence relate to MIS 12 (478–424 ka). In the Alpine region, Middle Pleistocene stratigraphies vary regionally and are fragmentary, but in northern and western Europe MIS 12 correlates with the large glaciation of the Elsterian (Cohen and Gibbard, 2019). According to our interpretation, Unit IX likely comprises soil material reworked by slope wash. Based on the susceptibility data it likely contains components of a well-developed interglacial soil, which would be pre-Elsterian (possibly Cromerian). The age of 413 ± 36 ka (KÖN-B-250) for Unit VIII on top of Unit IX may represent the MISs 12–11 boundary, as ongoing sedimentation and rather weak pedogenesis appear less likely for an interglacial (MIS 11). Based on geochronology and palaeosol morphology, there is no evidence for an MIS 11 palaeosol in the studied part of the Köndringen outcrop; it may have been eroded subsequent to its formation.

In Unit VII (profile KÖN-B), two consistent pIR-200 ages of 310 ± 25 ka (KÖN-C-130) and 306 ± 28 ka (KÖN-C-70) point towards deposition during MIS 9 (337–300 ka). Both ages are from a well-developed Bt horizon, most likely formed during interglacial conditions; therefore some rejuvenation by bioturbation or a slight age underestimation can be assumed. The highly calcareous loess of Unit VI has an age of 242 ± 18 ka (KÖN-B-340) and hence correlates with MIS 8 (300–243 ka). The age determined for the well-developed Bt horizon Unit V (160 ± 12 ka, KÖN-C-210) likely reflects the age of the parent material deposited during MIS 6 (191–130 ka), whereas soil formation presumably occurred during MIS 5e (130–115 ka), the Last Interglacial period (Eemian). Two pIR-200 ages determined for the upper PSU (Unit IV) of 119 ± 9 ka (KÖN-B-390) and 105 ± 8 ka (KÖN-C-290) fall into earlier phases of MIS 5 and likely

correspond to the beginning of the last glacial period during MIS 5d (115–102 ka). The two topmost samples taken from loess above (Unit III) have ages of 94 ± 7 ka (KÖN-B-470) and 93 ± 7 ka (KÖN-C-370), indicating deposition during MIS 5c (102–92 ka) to MIS 5b (92–85 ka).

Ln / Tn values from IRSL screening determined for the lower part of section KÖN-C do not reflect the hiatus between units X and VII that is clearly observed by the pIR-200 ages (505 ± 43 ka versus 310 ± 25 ka and 306 ± 28 ka). In this context, it has to be noted that Ln / Tn values have been determined using IRSL stimulated at $50\,^{\circ}$C, hence with a signal that will be affected by fading. In the presence of fading, the latent IRSL signal will rise to an equilibrium point at which the amount of newly produced latent signal equals the decay of the latent signal. This equilibrium point will be defined by the number of electron traps that host the latent signal, the fading rate, and the signal production rate, i.e. dose rate. The latter effect is reflected by the observation that the Ln / Tn values for the basal loess (units XI and X) are lower than those observed for the rest of the sequence. In fact, the dose rate in this part is lower (ca. $2.8\,\mathrm{Gy\,kyr^{-1}}$) compared to other parts of the sequence (ca. 3.7–$3.8\,\mathrm{Gy\,kyr^{-1}}$), which appear to be in equilibrium. In the present setting, the IRSL screening values carry age information only up to ca. 300 ka.

In the upper part of section KÖN-B, additional chronological information is derived from IRSL screening values that is not provided by the dating itself. First, Unit VI is clearly subdivided into a lower and upper subunit, as indicated by the offset in Ln / Tn values (7.59 ± 0.46 versus 6.20 ± 0.35). Such a significant offset may represent a time of several hundreds of thousands of years; hence, the lower part may correspond to MIS 10 (374–337 ka) and the upper part to MIS 8 (300–243 ka), the latter age being confirmed by a pIR-200 age. The continuation of Ln / Tn values just above and in Unit IV reveals that this part of the sequence was likely also deposited during MIS 8 but overprinted by later soil development. The gradual decrease in values from 8.14 ± 0.41 (160–180 cm) to 6.16 ± 0.16 (230 cm) implies quasi-continuous accumulation in the upper part of the investigated sequence. Apparently, continuous deposition is also observed for the upper part of Unit V in section KÖN-C, and it is shown that the lower part of this unit developed on older material (of Unit VII?). Unit IV and its subunits in this section apparently represent episodic deposition reflected by the different mean Ln / Tn values (Unit IVd: 6.01 ± 0.26; Unit IVc: 5.72 ± 0.24; Unit IVb and lower Unit IVa: 5.61 ± 0.10; Unit IVa: 5.43 ± 0.14). However, since dosimetric effects cannot be ruled out, this statement has to be treated with caution and would require proof by full dating.

From a magnetostratigraphic perspective, we note that the magnetic signatures of the Bt horizons related to MIS 9 and MIS 5 are not as high as those typically are for full interglacial conditions, but URG loess seems to have overall lower χ values than other Central European LPSs. As noted

previously (e.g. Necula et al., 2015; Marković et al., 2015), χ values of interglacial soils vary considerably in Europe. Furthermore, the type of pedogenesis and the position in the soil profile apparently influence this proxy. More geographically distributed χ data are necessary to understand the spatial pattern of the proxy intensities.

5.3   Stratigraphic context

During the past decades, research on LPSs in Central Europe has mainly focused on last glacial records, occasionally with obtained ages below Eemian palaeosols (e.g. Kadereit et al., 2013; Moine et al., 2017; Fischer et al., 2021; Lehmkuhl et al., 2016; Zens et al., 2018; Krauss et al., 2018; Rahimzadeh et al., 2021). Many Middle Pleistocene LPSs still lack state-of-the-art chronologies for individual loess and soil units, although palaeomagnetism and tephra stratigraphy are being applied where time intervals and material are present (e.g. Jordanova et al., 2022; Laag et al., 2021; Marković et al., 2015). TL ages from pre-Eemian (MIS 6 and older) loess elaborated during the 1980s to 1990s provide first approximations to the Middle Pleistocene loess chronology, though with large uncertainties (Zöller et al., 1988; Frechen et al., 1992; Frechen, 1994). IRSL ages from the late 1990s to early 2010s provide more robust estimates back to 200–250 ka (e.g. Preusser and Fiebig, 2009) at the LPS Wels-Aschet, Upper Austria. Further methodological advances are related to the application of thermally transferred (TT) OSL (Moska and Bluszcz, 2013) and pIR protocols (Schmidt et al., 2011a, b; Thiel et al., 2011a, b). Post-IR IRSL$_{290}$ dating, for example, extended the numerical age range in loess from Lower Austria (Paudorf, Göttweig-Furth and Aigen, Krems shooting range) and Hungary (Paks brickyard) to 300–350 ka (Thiel et al., 2011b, 2014; Sprafke et al., 2014; Sprafke, 2016). The MET-pIR ages determined at Köndringen reach back to 500 ka and are among the oldest luminescence ages obtained from loess in Central Europe. The opportunity to date back to pre-Holsteinian (MIS 11) times is promising from a geochronological point of view; however, pedostratigraphic relations at Köndringen are rather complicated and provide limited support to assess the reliability of our data in the absence of independent numerical age control.

A central controversy in loess research of Central Europe surrounds the questions of if Luvisols are strictly limited to full interglacial conditions and if these recurred every ca. 100 000 years, as proposed by Bibus (2002) for SW Germany and adopted by Terhorst et al. (2007, 2015) for Upper Austria. This hypothesis is apparently supported by LPSs in NW France, where Antoine et al. (2021) report seven interglacial Bt horizons between the surface soil and the Matuyama–Brunhes boundary (MBB) around 780 ka. However, at the LPS Weilbach (Hesse) it appears that MIS 7 is only represented by two humic horizons (Weilbacher Humuszonen), and the next Bt horizon below the Eemian palaeosol may rather correspond to MIS 9 (Schmidt et al., 2011b). At

Harmignies in Belgium, MIS 7 may be represented by two Bt horizons of Luvisols (Haesaerts et al., 2019), similar to findings from Červený kopec (Kukla, 1977) and other localities in Central Europe (e.g. Necula et al., 2015, and references therein). At Wels-Aschet, luminescence ages point to more than one Bt horizon being equivalent to MIS 7, consistent with two prominent global warm phases separated by a cooler phase encompassing MIS 7 (Preusser and Fiebig, 2009). At Koblenz-Metternich a formation of Luvisols reportedly occurred during pronounced interstadial conditions of the early Wurmian (Boenigk and Frechen, 2001). All the mentioned LPSs lack numerical age control by state-of-the-art methods, and there are further prominent LPSs in Central Europe that contain several fossil Bt horizons but lack a robust chronological framework for the Middle Pleistocene parts, for example Kärlich (Boenigk and Frechen, 1998), Bad Soden (Semmel and Fromm, 1976), Kirchheim (Rösner, 1990), Hagelstadt (Strunk, 1990), and Achenheim (Junkmanns, 1995). In summary, considering the discrepancies in Middle Pleistocene loess stratigraphy of Central Europe, it appears mandatory to date several geographically distributed LPSs with state-of-the-art luminescence dating approaches and precisely determine pathways of palaeopedogenesis to understand the regional imprint of spatially distinct palaeoclimates to the pedosphere (Sprafke, 2016).

At Köndringen, there are too many discontinuities to support or disprove available stratigraphic models. The two well-developed Bt horizons correspond to MISs 5e and 9, which suggests that these Luvisol subsoils represent full interglacial conditions. This is in agreement with earlier assumptions of Bronger (1966) and Guenther (1987), who suggest that regional interglacials are typically represented by Luvisols yet without being backed up by numeric age control. Some clay translocation in early glacial pedosediments of Unit IV in KÖN-C is likely related to a remobilisation of illuvial clay after post-Eemian colluviation in the absence of carbonate, as reported for the LPS Schatthausen near Heidelberg (Frechen et al., 2007). Interestingly in KÖN-B, there are no signs of clay translocation in the brown early glacial pedosediments, which may relate to some admixture of carbonate during colluviation, which hampers posterior clay translocation, as suggested for the MIS 5 pedocomplex of the LPS Paudorf, Lower Austria (Sprafke et al., 2014). This underlines that palaeoclimatic inferences from polygenetic and partly reworked palaeosols are difficult and require detailed (chrono-)stratigraphic, sedimentological, and also micromorphological studies. The lack of (micro-)morphological data is obvious with respect to the lower PSU at Köndringen, which is most likely an Elsterian pedosediment (see Sect. 5.2), with incipient interstadial pedogenesis in the lowermost and upper part. Advanced interglacial pedogenesis has most likely occurred before soil reworking, which would be pre-Elsterian (MIS 12), i.e. Cromerian. Thus, a Holsteinian palaeosol in other parts of the outcrop and/or in other sites of the region may be expected. The well-developed carbonate nod-

ules likely represent one or more Cromerian interglacials and are possibly the result of a merged soil developed during MISs 15–13, as interpreted for Central Europe (Terhorst, 2007; Bronger, 2003; Marković et al., 2015; Necula et al., 2015, and references therein).

The loess package between the upper and lower PSUs corresponds to MIS 8, which is known for rather little global ice volume compared to MISs 6, 10, and 12 (Lisiecki and Raymo, 2005). If loess volume is taken as an indicator for upstream glacier activity, the presence of a distinct MIS 8 loess package would imply a major phase of glaciation at this time. However, this period is usually not considered to represent full glacial conditions in the Alps (e.g. van Husen and Reitner, 2011), although it represents the phase of coldest sea surface temperatures of the last 1 million years at the Iberian Margin (Rodrigues et al., 2017, and references therein). Even in northern Switzerland, where one of the most complex glaciation histories has been reconstructed, there is still no unequivocal evidence for a major glaciation during MIS 8 (Preusser et al., 2011). Investigating further LPSs from the southern part of the URG, which is located downstream of the formerly glaciated areas of northern Switzerland, could give insight into aeolian sediment flux that is usually interpreted as a glacial signal in this region.

6   Conclusions

The studied section of the LPS Köndringen consists of loess sediments intercalated by two prominent pedosedimentary units (PSUs), of which the upper one is inclined to the west, cutting into the underlying loess and merging with the lower PSU. The applied high-resolution multi-method approach leads to detailed stratigraphic information and supports the reconstruction of the main phases of dust deposition, pedogenesis, and reworking of those units which were not lost by erosion. MET-pIR ages reach back to more than 500 ka and thus are among the oldest numerical ages obtained from loess in Central Europe. Massive carbonate concretions in the loess below the lower PSU point to advanced (interglacial) pedogenesis, apparently supported by the brownish colour, lack of carbonates, and higher clay contents in the lower PSU. However, the partly layered appearance, a weak pedogenic structure, and low χ values suggest at most interstadial pedogenesis. Temperature-dependent χ results support the assumption that the lower PSU contains reworked interglacial palaeosol material. Soil formation likely occurred during MIS 13 (and/or MIS 15?) and reworking during MIS 12 (Elsterian). The merged PSU in the western part of the studied outcrop comprises two well-developed interglacial Luvisol remnants (Bt horizons) dating to MIS 9 and MIS 5e (Eemian). Superimposed is a humic palaeosol with incipient clay coatings and the highest χ values likely formed during MIS 5c. As the LPS Köndringen contains several hiatuses and polygenetic units, the contribution towards refining the

Central European Middle Pleistocene loess stratigraphy remains limited for the time being. However, our study motivates future studies in the region using the applied multi-method approach in combination with MET-pIR state-of-the-art dating. Future studies on loess stratigraphy and chronology in the southern URG will contribute towards a better understanding of the chronology and impact of Alpine glaciations.

Data availability. Relevant data are given either in the main text or in the Supplement.

Supplement. The supplement related to this article is available online at: https://doi.org/10.5194/egqsj-72-1-2023-supplement.

References

Abdulkarim, M., Grema, H. M., Adamu, I. H., Mueller, D., Schulz, M., Ulbrich, M., Miocic, J. M., and Preusser, F.: Effect of using different chemical dispersing agents in grain size analyses of fluvial sediments via laser diffraction spectrometry, Methods Protoc., 4, 44, https://doi.org/10.3390/mps4030044, 2021.

Andres, W., Bos, J. A. A., Houben, P., Kalis, A. J., Nolte, S., Rittweger, H., and Wunderlich, J.: Environmental change and fluvial activity during the Younger Dryas in central Germany, Quatern. Int., 79, 89–100, https://doi.org/10.1016/S1040-6182(00)00125-7, 2001.

Antoine, P., Rousseau, D.-D., Moine, O., Kunesch, S., Hatte, C., Lang, A., Tissoux, H., and Zöller, L.: Rapid and cyclic aeolian deposition during the Last Glacial in European loess: a high-resolution record from Nussloch, Germany, Quaternary Sci. Rev., 28, 2955–2973, https://doi.org/10.1016/j.quascirev.2009.08.001, 2009.

Antoine, P., Coutard, S., Bahain, J. J., Locht, J. L., Hérisson, D., and Goval, E.: The last 750 ka in loess–palaeosol sequences from northern France: environmental background and dating of the western European Palaeolithic, J. Quaternary Sci., 36, 1293–1310, https://doi.org/10.1002/jqs.3281, 2021.

Bibus, E.: Abtragungs- und Bodenbildungsphasen im Rißlöß, E&G Quaternary Sci. J., 25, 166–182, https://doi.org/10.3285/eg.25.1.14, 1974.

Bibus, E.: Zum Quartär im mittleren Neckarraum – Reliefentwicklung, Löß/Paläobodensequenzen, Paläoklima, Tübinger Geowissenschaftliche Arbeiten, D8, 236 pp., ISBN 3-88121-055-5, 2002.

Boenigk, W. and Frechen, M.: Zur Geologie der Deckschichten von Kärlich/Mittelrhein, E&G Quaternary Sci. J., 48, 38–49, https://doi.org/10.3285/eg.48.1.04, 1998.

Boenigk, W. and Frechen, M.: The loess record in sections at Koblenz–Metternich and Tönchesberg in the Middle Rhine Area, Quatern. Int., 76, 201–209, https://doi.org/10.1016/S1040-6182(00)00103-8, 2001.

Bronger, A.: Lösse, ihre Verbraunungszonen und fossilen Böden. Ein Beitrag zur Stratigraphie des oberen Pleistozäns in Südbaden, Schriften des Geographischen Instituts der Universität Kiel 24/2, Geographisches Institut der Universität Kiel, Kiel, 113 pp., 1966.

Bronger, A.: Zur Klimageschichte des Quartärs von Südbaden auf bodengeographischer Grundlage, Petermann. Geogr. Mitt., 113, 112–124, 1969.

Bronger, A.: Zur Mikromorphogenese und zum Tonmineralbestand quartärer Lössböden in Südbaden, Geoderma, 3, 281–320, https://doi.org/10.1016/0016-7061(70)90011-X, 1970.

Bronger, A.: Correlation of loess-paleosol sequences in East and Central Asia with SE Central Europe: towards a continental Quaternary pedostratigraphy and paleoclimatic history, Quatern. Int., 106, 11–31, https://doi.org/10.1016/S1040-6182(02)00159-3, 2003.

Buylaert, J. P., Murray, A. S., Thomsen, K. J., and Jain, M.: Testing the potential of an elevated temperature IRSL signal from K-feldspar, Radiat. Meas., 44, 560–565, https://doi.org/10.1016/j.radmeas.2009.02.007, 2009.

Cohen, K. M. and Gibbard, P. L.: Global chronostratigraphical correlation table for the last 2.7 million years, version 2019 QI-500, Quatern. Int., 500, 20–31, https://doi.org/10.1016/j.quaint.2019.03.009, 2019.

Degering, D. and Degering, A.: Change is the only constant – Time-dependent dose rates in luminescence dating, Quat. Geochronol., 58, 101074, https://doi.org/10.1016/j.quageo.2020.101074, 2020.

EEA (European Environment Agency): European Digital Elevation Model (EU-DEM), version 1.1, Copernicus Land Monitoring Service 2016, European Union, https://land.copernicus.eu/imagery-in-situ/eu-dem/eu-dem-v1.1?tab=download (last access: 20 July 2022), 2016.

Ehlers, J., Gibbard, P. L., and Hughes, P. D. (Eds.): Quaternary Glaciations – Extent and Chronology A Closer Look, Developments in Quaternary Sciences, 15, Elsevier, 1108 pp., ISBN 978-0-444-53447-7, 2011.

Erkens, G., Dambeck, R., Volleberg, K. P., Bouman, M. T. I. J., Bos, J. A. A., Cohen, K. M., Wallinga, J., and Hoek, W. Z.: Fluvial terrace formation in the northern Upper Rhine Graben during the last 20000 years as a result of allogenic controls and autogenic evolution, Geomorphology, 103, 476–495, https://doi.org/10.1016/j.geomorph.2008.07.021, 2009.

Faershtein, G., Porat, N., and Matmon, A.: Natural saturation of OSL and TT-OSL signals of quartz grains from Nilotic origin, Quat. Geochronol., 49, 146–152, https://doi.org/10.1016/j.quageo.2018.04.002, 2019.

FAO (Food and Agriculture Organization of the United Nations): Guidelines for soil description. Food and Agriculture Organization of the United Nations, 4th edn., Roma, Italy, ISBN 92-5-105521-1, 2006.

Fischer, P., Jöris, O., Fitzsimmons, K., Vinnepand, M., Prud'homme, C., Schulte, P., Hatté, C., Hambach, U., Lindauer, S., Zeeden, C., Peric, Z., Lehmkuhl, F., Wunderlich, T., Wilken, D., Schirmer, W., and Vött, A.: Millennial-scale terrestrial ecosystem responses to Upper Pleistocene climatic changes: 4D-reconstruction of the Schwalbenberg Loess-Palaeosol-Sequence (Middle Rhine Valley, Germany), Catena, 196, 104913, https://doi.org/10.1016/j.catena.2020.104913, 2021.

Frechen, M.: Systematic Thermoluminescence Dating of 2 Loess Profiles from the Middle Rhine Area (F.R.G.), Quaternary Sci. Rev., 11, 93–101, https://doi.org/10.1016/0277-3791(92)90048-D, 1992.

Frechen, M.: Thermolumineszens-Datierungen an Lössen des Tönchesberges aus der Osteifel, E&G Quaternary Sci. J., 44, 79–93, https://doi.org/10.3285/eg.44.1.08, 1994.

Frechen, M., Brückner, H., and Radtke, U.: A comparison of different TL-techniques on loess samples from Rheindahlen (FRG), Quaternary Sci. Rev., 11, 109–113, https://doi.org/10.1016/0277-3791(92)90050-I, 1992.

Frechen, M., Terhorst, B., and Rähle, W.: The Upper Pleistocene loess/palaeosol sequence from Schatthausen in North Baden-Württemberg, E&G Quaternary Sci. J., 56, 212–227, https://doi.org/10.3285/eg.56.3.05, 2007.

Gabriel, G., Ellwanger, D., Hoselmann, C., Weidenfeller, M., Wielandt-Schuster, U., and The Heidelberg Basin Project Team: The Heidelberg Basin, Upper Rhine Graben (Germany): a unique archive of Quaternary sediments in Central Europe, Quatern. Int., 292, 43–58, https://doi.org/10.1016/j.quaint.2012.10.044, 2013.

Galbraith, R. F., Roberts, R. G., Laslett, G. M., Yoshida, H., and Olley, J. M.: Optical Dating of single and multiple Grains of

Quartz from Jinmium Rock Shelter, Northern Australia: Part I, Experimental Design and Statistical Models, Archaeometry, 41, 2, 339–364, 1999.

Guenther, E. W.: Sedimentpetrographische Untersuchung von Lössen-Zur Gliederung des Eiszeitalters und zur Einordnung paläolithischer Kulturen, Teil 1 Methodische Grundlagen mit Erläuterung an Profilen, Böhlau Verlag Köln Graz, p. 10, 1961.

Guenther, E. W.: Zur Gliederung der Lösse des südlichen Oberrheintals, E&G Quaternary Sci. J., 37, 67–78, https://doi.org/10.3285/eg.37.1.07, 1987.

Hädrich, F.: Die Böden der Emmendinger Vorbergzone (Südliches Oberrheingebiet), Berichte der Naturforschenden Gesellschaft Freiburg i. Br., 56, 23–76, 1965.

Hädrich, F.: Zur Methodik der Lößdifferenzierung auf der Grundlage der Carbonatverteilung, E&G Quaternary Sci. J., 26, 95–117, https://doi.org/10.3285/eg.26.1.06, 1975.

Hädrich, F.: Paläoböden im südlichen Oberrhein Gebiet, Berichte der Naturforschenden Gesellschaft Freiburg i. Br., 70, 29–48, 1980.

Hädrich, F. and Lamparski, F.: Ein rißzeitlicher Eiskeil im Lößaufschluß von Buggingen (Südbaden) mit einem Beitrag zur Lößkindelgenese, Berichte der Naturforschenden Gesellschaft Freiburg i. Br., 74, 25–47, 1984.

Hädrich, F. and Stahr, K.: Die Böden des Breisgaus und angrenzender Gebiete, Berichte der Naturforschenden Gesellschaft Freiburg i. Br., 91., 148 pp., 2001.

Haesaerts, P., Dupuis, C., Spagna, P., Damblon, F., Balescu, S., Jadin, I., Lavachery, P., Pirson, S., and Bosquet, D.: Révision du cadre chronostratigraphique des assemblages Levallois issus des nappes alluviales du Pléistocène moyen dans le bassin de la Haine (Belgique), in: Actes du XXVIIIe Congrès Préhistorique de France, Amiens, France, 30 May–4 June 2016, Société préhistorique de France, Paris, France, 179–199, 2019.

Heiri, O., Lotter, A. F., and Lemcke, G.: Loss on ignition as a method for estimating organic and carbonate content in sediments: reproducibility and comparability of results, J. Paleolimnol., 25, 101–110, https://doi.org/10.1023/A:1008119611481, 2001.

Heiri, O., Koinig, K. A., Spötl, C., Barrett, S., Brauer, A., Drescher-Schneider, R., Gaar, D., Ivy-Ochs, S., Kerschner, H., Luetscher, M., Moran, A., Nicolussi, K., Preusser, F., Schmidt, R., Schoeneich, P., Schwörer, C., Sprafke, T., Terhorst, B., and Tinner, W.: Palaeoclimate records 60–8 ka in the Austrian and Swiss Alps and their forelands, Quaternary Sci. Rev., 106, 186–205, https://doi.org/10.1016/j.quascirev.2014.05.021, 2014.

Hofmann, F. M., Rauscher, F., McCreary, W., Bischoff, J.-P., and Preusser, F.: Revisiting Late Pleistocene glacier dynamics northwest of the Feldberg, southern Black Forest, Germany, E&G Quaternary Sci. J., 69, 61–87, https://doi.org/10.5194/egqsj-69-61-2020, 2020.

Houben, P.: Spatio-temporally variable response of fluvial systems to Late Pleistocene climate change: a case study from central Germany, Quaternary Sci. Rev., 22, 2125–2140, https://doi.org/10.1016/S0277-3791(03)00181-1, 2003.

Huntley, D. J. and Baril, M. R.: The K content of the K-feldspars being measured in optical dating or in thermoluminescence dating, Ancient TL, 15, 11–13, 1997.

Jordanova, D., Laag, C., Jordanova, N., Lagroix, F., Georgieva, B., Ishlyamski, D., and Guyodo, Y.: A detailed magnetic record of Pleistocene climate and distal ash dispersal during the last 800 kyrs – The Suhia Kladenetz quarry loess-paleosol sequence near Pleven (Bulgaria), Glob. Planet. Change, 214, 103840, https://doi.org/10.1016/j.gloplacha.2022.103840, 2022.

Junkmanns, J.: Les ensembles lithiques d'Achenheim d'apres la collection de Paul Wernert, Bull. Soc. Préhist. Fr., 92, 26–36, 1995.

Kadereit, A., Kind, C.-J., and Wagner, G. A.: The chronological position of the Lohne Soil in the Nussloch loess section – re-evaluation for a European loess-marker horizon, Quaternary Sci. Rev., 59, 67–86, https://doi.org/10.1016/j.quascirev.2012.10.026, 2013.

Kars, R. H., Reimann, T., Ankjærgaard, C., and Wallinga, J.: Bleaching of the post-IR IRSL signal: new insights for feldspar luminescence dating, Boreas, 43, 780–791, https://doi.org/10.1111/bor.12082, 2014.

Keßler, G. and Laiber, J.: Erläuterungen zu Blatt 7813 Emmendingen, Geologisches Landesamt Baden-Württemberg, Landesvermessungsamt Baden-Württemberg, Stuttgart, 1991.

Kleinmann, A., Müller, H., Lepper, J., and Waas, D.: Nachtigall: A continental sediment and pollen sequence of the Saalian Complex in NW-Germany and its relationship to the MIS-framework, Quatern. Int., 241, 97–110, https://doi.org/10.1016/j.quaint.2010.10.005, 2011.

Knipping, M.: Early and Middle Pleistocene pollen assemblages of deep core drillings in the northern Upper Rhine Graben, Germany, Neth. J. Geosci., 87, 51–65, https://doi.org/10.1017/S0016774600024045, 2008.

Kock, S., Huggenberger, P., Preusser, F., Rentzel., P., and Wetzel, A.: Formation and evolution of the Lower Terrace of the Rhine River in the area of Basel, Swiss J. Geosci. 102, 307–321, https://doi.org/10.1007/s00015-009-1325-1, 2009.

Konert, M. and Vandenberghe, J.: Comparison of laser grain size analysis with pipette and sieve analysis: a solution for the underestimation of the clay fraction, Sedimentology, 44, 523–535, https://doi.org/10.1046/j.1365-3091.1997.d01-38.x, 1997.

Krauss, L., Kappenberg, A., Zens, J., Kehl, M., Schulte, P., Zeeden, C., Eckmeier, E., and Lehmkuhl, F.: Reconstruction of Late Pleistocene paleoenvironments in southern Germany using two high-resolution loess-paleosol records, Palaeogeogr. Palaeocl., 509, 58–76, https://doi.org/10.1016/j.palaeo.2017.11.043, 2018.

Kukla G. J.: Pleistocene land-sea correlations. 1: Europe. Earth-Sci. Rev., 13, 307–374, https://doi.org/10.1016/0012-8252(77)90125-8, 1977.

Laag C., Hambach U., Zeeden C., Lagroix F., Guyodo Y., Veres V., Jovanović M., and Marković S. B.: A Detailed Paleoclimate Proxy Record for the Middle Danube Basin Over the Last 430 kyr: A Rock Magnetic and Colorimetric Study of the Zemun Loess-Paleosol Sequence, Front. Earth Sci., 9, 600086, https://doi.org/10.3389/feart.2021.600086, 2021.

Lehmkuhl, F., Zens, J., Krauß, L., Schulte, P., and Kels, H.: Loess-palaeosol sequences at the northern European loess belt in Germany: Distribution, geomorphology and stratigraphy, Quaternary Sci. Rev., 153, 11–30, https://doi.org/10.1016/j.quascirev.2016.10.008, 2016.

Lehmkuhl, F., Nett, J. J., Pötter, S., Schulte, P., Sprafke, T., Jary, Z., Antoine, P., Wacha, L., Wolf, D., Zerboni, A., Hošek, J., Marković, S. B., Obreht, I., Sümegi, P., Veres, D., Zeeden, C., Boemke, B., Schaubert, V., Viehweger, J., and Ham-

bach, U.: Loess landscapes of Europe – Mapping, geomorphology, and zonal differentiation, Earth-Sci. Rev., 215, 103496, https://doi.org/10.1016/j.earscirev.2020.103496, 2021.

Li, B. and Li, S.-H.: Luminescence dating of K-feldspar from sediments: A protocol without anomalous fading correction, Quat. Geochronol, 6, 468–479, https://doi.org/10.1016/j.quageo.2011.05.001, 2011.

Li, Y., Tsukamoto, S., Frechen, M., and Gabriel, G.: Timing of fluvial sedimentation in the Upper Rhine Graben since the Middle Pleistocene: constraints from quartz and feldspar luminescence dating, Boreas, 47, 256–270, https://doi.org/10.1111/bor.12266, 2018.

Lisiecki, L. E. and Raymo, M. E.: A Pliocene-Pleistocene stack of 57 globally distributed benthic δ^{18}O records, Paleoceanography, 20, PA1003, https://doi.org/10.1029/2004PA001071, 2005.

Lowick, S. E., Trauerstein, M., and Preusser, F.: Testing the application of post IR-IRSL dating to fine grain waterlain sediments, Quat. Geochronol., 8, 33–40, https://doi.org/10.1016/j.quageo.2011.12.003, 2012.

Marković, S. B., Stevens, T., Kukla, G. J., Hambach, U., Fitzsimmons, K. E., Gibbard, P., Buggle, B., Zech, M., Guo, Z., Hao, Q., Wu, H., O'Hara Dhand, K., Smalley, I. J., Újvári, G., Sümegi, P., Timar-Gabor, A., Veres, D., Sirocko, F., Vasiljević, D. A., Jary, Z., Svensson, A., Jović, V., Lehmkuhl, F., Kovács, J., and Svirčev, Z.: Danube loess stratigraphy – Towards a pan-European loess stratigraphic model, Earth-Sci. Rev., 148, 228–258, https://doi.org/10.1016/j.earscirev.2015.06.005, 2015.

May, J.-H., Marx, S. K., Reynolds, W., Clark-Balzan, L., Jacobsen, G. E., and Preusser, F.: Establishing a chronological framework for a late Quaternary seasonal swamp in the Australian "Top End", Quat. Geochronol., 47, 81–92, https://doi.org/10.1016/j.quageo.2018.05.010, 2018.

Mercier, J.-L. and Jeser, N.: The glacial history of the Vosges Mountains, Developments in Quaternary Science, 2,113–118, https://doi.org/10.1016/S1571-0866(04)80061-7, 2004.

Meszner, S., Kreutzer, S., Fuchs, M., and Faust, D.: Late Pleistocene landscape dynamics in Saxony, Germany: Paleoenvironmental reconstruction using loess-paleosol sequences, Quatern. Int., 296, 94–107, https://doi.org/10.1016/j.quaint.2012.12.040, 2013.

Meyers, P. A. and Lallier-Verges, E.: Lacustrine sedimentary organic matter records of Late Quaternary paleoclimates, J. Paleolimnol., 21, 345–372, https://doi.org/10.1023/A:1008073732192, 1999.

Moine, O., Antoine, P., Hatté, C., Landais, A., Mathieu, J., Prud'homme, C., and Rousseau, D.-D.: The impact of Last Glacial climate variability in west-European loess revealed by radiocarbon dating of fossil earthworm granules, P. Natl. Acad. Sci. USA, 114, 6209–6214, https://doi.org/10.1073/pnas.1614751114, 2017.

Moska, P. and Bluszcz, A.: Luminescence dating of loess profiles in Poland, Quatern. Int., 296, 51–60, https://doi.org/10.1016/j.quaint.2012.09.004, 2013.

Necula, C., Dimofte, D., and Panaiotu, C.: Rock magnetism of a loess-palaeosol sequence from the western Black Sea shore (Romania), Geophys. J. Int., 202, 1733–1748, https://doi.org/10.1093/gji/ggv250, 2015.

Pécsi, M. and Richter, G.: Löss: Herkunft – Gliederung – Landschaften, Z. Geomorphol., N.F., Supplementband 98, Bornträger, Berlin & Stuttgart, 391 pp., ISBN 3-443-21098-8, 1996.

Prescott, J. R. and Hutton, J. T.: Cosmic ray contributions for dose rates for luminescence and ESR dating: Large depths and long-term time variations, Radiat. Meas., 23, 497–500, https://doi.org/10.1016/1350-4487(94)90086-8, 1994.

Preusser, F.: Towards a chronology of the Late Pleistocene in the northern Alpine Foreland, Boreas, 33, 195–210, https://doi.org/10.1111/j.1502-3885.2004.tb01141.x, 2004.

Preusser F. and Fiebig M.: European Middle Pleistocene loess chronostratigraphy: Some considerations based on evidence from the Wels site, Austria, Quatern. Int., 198, 37–45, https://doi.org/10.1016/j.quaint.2008.07.006, 2009.

Preusser, F., Drescher-Schneider, R., Fiebig, M., and Schlüchter, C.: Re-interpretation of the Meikirch pollen record, Swiss Alpine Foreland, and implications for Middle Pleistocene chronostratigraphy, J. Quaternary Sci., 20, 607–620, https://doi.org/10.1002/jqs.930, 2005.

Preusser, F., Graf, H. R., Keller, O., Krayss, E., and Schlüchter, C.: Quaternary glaciation history of northern Switzerland, E&G Quaternary Sci. J., 60, 21, https://doi.org/10.3285/eg.60.2-3.06, 2011.

Preusser, F., Büschelberger, M., Kemna, H. A., Miocic, J., Mueller, D., and May, J.-H.: Quaternary aggradation in the Upper Rhine Graben linked to the glaciation history of northern Switzerland, Int. J. Earth Sci., 110, 1827–1846, https://doi.org/10.1007/s00531-021-02043-7, 2021.

Qin, J., Chen, J., Li, Y., and Zhou, L.: Initial sensitivity change of K-feldspar pIRIR signals due to uncompensated decrease in electron trapping probability: evidence from radiofluorescence measurements, Radiat. Meas., 120, 131–136, https://doi.org/10.1016/j.radmeas.2018.06.017, 2018.

Rahimzadeh, N., Sprafke, T., Thiel, C., Terhorst, B., and Frechen, M.: A comparison of polymineral and K-feldspar post-infrared infrared stimulated luminescence ages of loess from Franconia, southern Germany, E&G Quaternary Sci. J., 70, 53–71, https://doi.org/10.5194/egqsj-70-53-2021, 2021.

Rees-Jones, J.: Optical Dating Of Young Sediments Using Fine-Grain Quartz, Ancient TL, 13, 9–14, 1995.

Richter, D., Richter, A., and Dornich, K.: Lexsyg smart – a luminescence detection system for dosimetry, material research and dating application, Geochronometria, 42, 202–209, https://doi.org/10.1515/geochr-2015-0022, 2015.

Roberts, H. M., Durcan, J. A., and Duller, G. A. T.: Exploring procedures for the rapid assessment of optically stimulated luminescence range-finder ages, Radiat. Meas., 44, 582–587, https://doi.org/10.1016/j.radmeas.2009.02.006, 2009.

Rodrigues, T., Alonso-García, M., Hodell, D. A., Rufino, M., Naughton, F., Grimalt, J. O., Voelker, A. H. L., and Abrantes, F.: A 1-Ma record of sea surface temperature and extreme cooling events in the North Atlantic: A perspective from the Iberian Margin, Quaternary Sci. Rev., 172, 118–130, https://doi.org/10.1016/j.quascirev.2017.07.004, 2017.

Rösner, U.: Die Mainfränkische Lößprovinz. Sedimentologische, pedologische und morphodynamische Prozesse der Lößbildung währenddes Pleistozäns in Mainfranken, Erlanger Geographische Arbeiten, 301 pp., 1990.

Schmidt, E. D., Frechen, M., Murray, A. S., Tsukamoto, S., and Bittmann, F.: Luminescence chronology of the loess record from the Tönchesberg section: A comparison of using quartz and feldspar as dosimeter to extend the age range beyond the Eemian, Quatern. Int., 234, 10–22, https://doi.org/10.1016/j.quaint.2010.07.012, 2011a.

Schmidt, E. D., Semmel, A., and Frechen, M.: Luminescence dating of the loess/palaeosol sequence at the gravel quarry Gaul/Weilbach, Southern Hesse (Germany), E&G Quaternary Sci. J., 60, 9, https://doi.org/10.3285/eg.60.1.08, 2011b.

Scholger, R. and Terhorst, B.: Magnetic excursions recorded in the Middle to Upper Pleistocene loess/palaeosol sequence Wels-Aschet (Austria), E&G Quaternary Sci. J., 62, 14–21, https://doi.org/10.3285/eg.62.1.02, 2013.

Schulte, P. and Lehmkuhl, F.: The difference of two laser diffraction patterns as an indicator for post-depositional grain size reduction in loess-paleosol sequences, Palaeogeogr. Palaeocl., 509, 126–136, https://doi.org/10.1016/j.palaeo.2017.02.022, 2018.

Schulte, P., Sprafke, T., Rodrigues, L., and Fitzsimmons, K. E.: Are fixed grain size ratios useful proxies for loess sedimentation dynamics? Experiences from Remizovka, Kazakhstan, Aeolian Res., 31, 131–140, https://doi.org/10.1016/j.aeolia.2017.09.002, 2018.

Schulze, T., Schwahn, L., Fülling, A., Zeeden, C., Preusser, F., and Sprafke, T.: Investigating the loess–palaeosol sequence of Bahlingen-Schönenberg (Kaiserstuhl), southwestern Germany, using a multi-methodological approach, E&G Quaternary Sci. J., 71, 145–162, https://doi.org/10.5194/egqsj-71-145-2022, 2022.

Semmel, A.: Studien über den Verlauf jungpleistozäner Formung in Hessen, Frankfurter geographische Hefte, 44, 1–133, 1968.

Semmel, A. and Fromm, K.: Ergebnisse paläomagnetischer Untersuchungen an quartären Sedimenten des Rhein-Main-Gebiets, E&G Quaternary Sci. J., 27, 18–25, https://doi.org/10.3285/eg.27.1.02, 1976.

Smedley, R. K., Duller, G. A. T., and Roberts, H. M.: Bleaching of the post-IR IRSL signal from individual grains of K-feldspar: Implications for single-grain dating, Radiat. Meas., 79, 33–42, https://doi.org/10.1016/j.radmeas.2015.06.003, 2015.

Sprafke, T.: Löss in Niederösterreich – Archiv quartärer Klima- und Landschaftsveränderungen, Würzburg University Press, https://doi.org/10.25972/WUP-978-3-95826-039-9, 2016.

Sprafke, T. and Obreht, I.: Loess: Rock, sediment or soil – What is missing for its definition?, Quatern. Int., 399, 198–207, https://doi.org/10.1016/j.quaint.2015.03.033, 2016.

Sprafke, T., Thiel, C., and Terhorst, B.: From micromorphology to palaeoenvironment: The MIS 10 to MIS 5 record in Paudorf (Lower Austria), Catena, 117, 60–72, https://doi.org/10.1016/j.catena.2013.06.024, 2014.

Sprafke, T., Schulte, P., Meyer-Heintze, S., Händel, M., Einwögerer, T., Simon, U., Peticka, R., Schäfer, C., Lehmkuhl, F., and Terhorst, B.: Paleoenvironments from robust loess stratigraphy using high-resolution color and grain-size data of the last glacial Krems-Wachtberg record (NE Austria), Quaternary Sci. Rev., 248, 106602, https://doi.org/10.1016/j.quascirev.2020.106602, 2020.

Stebich, M., Höfer, D., Mingram, J., Nowaczyk, N., Rohrmüller, J., Mrlina, J., and Kämpf, H.: A contribution towards the palynostratigraphical classification of the Middle Pleistocene in Central Europe: The pollen record of the Neualbenreuth Maar, north-

eastern Bavaria (Germany), Quaternary Sci. Rev., 250, 106681, https://doi.org/10.1016/j.quascirev.2020.106681, 2020.

Stephan, H.-J.: Climato-stratigraphic subdivision of the Pleistocene in Schleswig-Holstein, Germany and adjoining areas: status and problems, E&G Quaternary Sci. J., 63, 3–18, https://doi.org/10.3285/eg.63.1.01, 2014.

Stojakowits P., Mayr C., Ivy-Ochs S., Preusser F., Reitner J., and Spötl C.: Environments at the MIS 3/2 transition in the northern Alps and their foreland, Quatern. Int., 581/582, 99–113, https://doi.org/10.1016/j.quaint.2020.08.003, 2021.

Strunk, H.: Das Quartärprofil von Hagelstadt im Bayerischen Tertiärhügelland, E&G Quaternary Sci. J., 40, 85–96, https://doi.org/10.3285/eg.40.1.06, 1990.

Terhorst, B.: Korrelation von mittelpleistozänen Löss-/Paläobodensequenzen in Oberösterreich mit einer marinen Sauerstoffisotopenkurve, E&G Quaternary Sci. J., 56, 172–185, https://doi.org/10.3285/eg.56.3.03, 2007.

Terhorst, B.: A stratigraphic concept for Middle Pleistocene Quaternary sequences in Upper Austria , E&G Quaternary Sci. J., 62, 4–13, https://doi.org/10.3285/eg.62.1.01, 2013.

Terhorst, B., Frechen, M., and Reitner, J.: Chronostratigraphische Ergebnisse aus Lößprofilen der Inn-und Traun-Hochterrassen in Oberösterreich, Z. Geomorphol., Supplementband, 127, 213–232, 2002.

Terhorst, B., Sedov, S., Sprafke, T., Peticzka, R., Meyer-Heintze, S., Kühn, P., and Solleiro Rebolledo, E.: Austrian MIS 3/2 loess–palaeosol records – Key sites along a west–east transect, Palaeogeogr. Palaeocl., 418, 43–56, https://doi.org/10.1016/j.palaeo.2014.10.020, 2015.

Thiel, C., Buylaert, J.-P., Murray, A. S., Terhorst, B., Hofer, I., Tsukamoto, S., and Frechen, M.: Luminescence dating of the Stratzing loess profile (Austria) – testing the potential of an elevated temperature post-IR IRSL protocol, Quatern. Int., 234, 23–31, https://doi.org/10.1016/j.quaint.2010.05.018, 2011a.

Thiel, C., Buylaert, J.-P., Murray, A. S., Terhorst, B., Tsukamoto, S., Frechen, M., and Sprafke, T.: Investigating the chronostratigraphy of prominent palaeosols in Lower Austria using post-IR IRSL dating, E&G Quaternary Sci. J., 60, 11, https://doi.org/10.3285/eg.60.1.10, 2011b.

Thiel, C., Terhorst, B., Jaburová, I., Buylaert, J. P., Murray, A. S., Fladerer, F. A., Damm, B., Frechen, M., and Ottner, F.: Sedimentation and erosion processes in Middle to Late Pleistocene sequences exposed in the brickyard of Langenlois/Lower Austria, Geomorphology, 135, 295–307, https://doi.org/10.1016/j.geomorph.2011.02.011, 2011c.

Thiel, C., Horvaìth, E., and Frechen, M.: Revisiting the loess/palaeosol sequence in Paks, Hungary: A post-IR IRSL based chronology for the "Young Loess Series", Quatern. Int., 319, 88–98, https://doi.org/10.1016/j.quaint.2013.05.045, 2014.

Tucci, M., Krahn, K.J., Richter, D., van Kolfschoten, T., Rodríguez Álvarez, B., Verheijen, I., Serangeli, J., Lehmann, J., Degering, D., Schwalb, A., and Urban, B.: Evidence for the age and timing of environmental change associated with a Lower Palaeolithic site within the Middle Pleistocene Reinsdorf sequence of the Schöningen coal mine, Germany, Palaeogeogr. Palaeocl., 569, 110309, https://doi.org/10.1016/j.palaeo.2021.110309, 2021.

Vandenberghe, J.: Grain size of fine-grained windblown sediment: A powerful proxy for process identification, Earth-Sci. Rev., 121, 18–30, https://doi.org/10.1016/j.earscirev.2013.03.001, 2013.

Van Husen, D. and Reitner, J. M.: An Outline of the Quaternary Stratigraphy of Austria, E&G Quaternary Sci. J., 60, 24, https://doi.org/10.3285/eg.60.2-3.09, 2011.

Viscarra Rossel, R. A., Walvoort, D. J. J., McBratney, A. B., Janik, L.J., and Skjemstad, J. O.: Visible, near infrared, mid infrared or combined diffuse reflectance spectroscopy for simultaneous assessment of various soil properties, Geoderma, 131, 59–75, https://doi.org/10.1016/j.geoderma.2005.03.007, 2006.

Weidenfeller, M. and Knipping, M.: Correlation of Pleistocene sediments from boreholes in the Ludwigshafen area, western Heidelberg Basin, E&G Quaternary Sci. J., 57, 270–285, https://doi.org/10.3285/eg.57.3-4.1, 2009.

Wintle, A. G. and Murray, A. S.: A review of quartz optically stimulated luminescence characteristics and their relevance in single-aliquot regeneration dating protocols, Radiat. Meas., 41, 369–391, https://doi.org/10.1016/j.radmeas.2005.11.001, 2006.

Zander, A. and Hilgers, A.: Potential and limits of OSL, TT-OSL, IRSL and pIRIR$_{290}$ dating methods applied on a Middle Pleistocene sediment record of Lake El'gygytgyn, Russia, Clim. Past, 9, 719–733, https://doi.org/10.5194/cp-9-719-2013, 2013.

Zeeden, C. and Hambach, U.: Magnetic susceptibility properties of loess from the Willendorf archaeological site: Implications for the syn/post-depositional interpretation of magnetic fabric, Front. Earth Sci., 8, 599491, https://doi.org/10.3389/feart.2020.599491, 2021.

Zeeden, C., Kels, H., Hambach, U., Schulte, P., Protze, J., Eckmeier, E., Markovic, S. B., Klasen, N., and Lehmkuhl, F.: Three climatic cycles recorded in a loess-palaeosol sequence at Semlac (Romania) – Implications for dust accumulation in south-eastern Europe, Quaternary Sci. Rev., 154, 130–142, https://doi.org/10.1016/j.quascirev.2016.11.002, 2016.

Zeeden, C., Mir, J. A., Vinnepand, M., Laag, C., Rolf, C., and Dar, R. A.: Local mineral dust transported by varying wind intensities forms the main substrate for loess in Kashmir, E&G Quaternary Sci. J., 70, 191–195, https://doi.org/10.5194/egqsj-70-191-2021, 2021.

Zens, J., Schulte, P., Klasen, N., Krauß, L., Pirson, S., Burow, C., Brill, D., Eckmeier, E., Kels, H., Zeeden, C., Spagna, P., and Lehmkuhl, F.: OSL chronologies of paleoenvironmental dynamics recorded by loess-paleosol sequences from Europe: Case studies from the Rhine-Meuse area and the Neckar Basin, Palaeogeogr. Palaeocl, 509, 105–125, https://doi.org/10.1016/j.palaeo.2017.07.019, 2018.

Zhang, J.: Behavior of the electron trapping probability change in IRSL dating of K-feldspar: A dose recovery study, Quat. Geochronol., 44, 38–46, https://doi.org/10.1016/j.quageo.2017.12.001, 2018.

Zhang, J. and Li, S.-H.: Review of the Post-IR IRSL Dating Protocols of K-Feldspar, Methods Protoc., 3, 7, https://doi.org/10.3390/mps3010007, 2020.

Zöller, L., Stremme, H., and Wagner, G.A.: Thermolumineszenz-Datierung an Löss-Paläoboden-Sequenzen von Nieder-, Mittel- und Oberrhein/Bundesrepublik Deutschland, Chem. Geol., 73, 39–62, https://doi.org/10.1016/0168-9622(88)90020-6, 1988.

Zöller, L., Fischer, M., Jary, Z., Antoine, P., and Krawczyk, M.: Chronostratigraphic and geomorphologic challenges of last glacial loess in Poland in the light of new luminescence ages, E&G Quaternary Sci. J., 71, 59–81, https://doi.org/10.5194/egqsj-71-59-2022, 2022.